Spring 2016

Behavior of hollow-core composite columns under torsion loading

Sujith Anumolu

Department:

BEHAVIOR OF HOLLOW-CORE COMPOSITE COLUMNS UNDER TORSION LOADING

by

SUJITH ANUMOLU

A THESIS

Presented to the Faculty of the Graduate School of the

MISSOURI UNIVERSITY OF SCIENCE AND TECHNOLOGY

In Partial Fulfillment of the Requirements for the Degree

MASTER OF SCIENCE

in

CIVIL ENGINEERING

2016

Approved by:

Mohamed A. ElGawady, Advisor
Guirong Grace Yan
K. Chandrashekhara

PUBLICATION DISSERTATION OPTION

This dissertation has been prepared in the style such that the individual sections may be submitted for publication in the *Journal of Bridge Engineering* published by the American Society of Civil Engineers (ASCE).

Paper I (pages 20-66) is a manuscript entitled "Behavior of Hollow-Core Steel-Concrete-Steel Columns Subjected to Torsion Loading." This manuscript was submitted for publication in the *Journal of ASCE Bridge Engineering*.

Paper II (pages 20-66) is a manuscript entitled "Torsion Behavior of Hollow-Core FRP-Concrete-Steel Columns." This manuscript was submitted for publication in the *Journal of ASCE Bridge Engineering*.

ABSTRACT

The effect of torsional loads could be significant along with axial and flexural loads on bridge columns during earthquake excitations. The present study presents the torsional behavior of hollow-core steel-concrete-steel columns (HC-SCS) and hollow-core fiber reinforced polymer-concrete-steel columns (HC-FCS). The HC-SCS comprises of sandwiched concrete shell between two steel tubes whereas in HC-FCS column, the outer steel tube of HC-SCS column was replaced by the FRP tube. Both columns have stay-in place permanent form-work to the concrete shell in the form of outer and inner tubes. The steel tubes serve as longitudinal and shear reinforcement to the column. Finite element models of HC-SCS columns were developed using LS-Dyna and the analysis results were validated with an average error of 4.8% against the experimental results in predicting the HC-SCS column's torsional capacity. An extensive parametric study was conducted with seven parameters to better understand the column's torsional behavior. A simplified analytical model was developed to predict the column's torsional capacity with an accuracy of 90%. A large-scale HC-FCS column was constructed and tested under constant axial load and cyclic torsion loading. The column outer diameter was 24 inch with an aspect ratio of 4. The FRP tube was placed on the surface of the footing while the steel tube was embedded into the footing to a length of 1.8 times the diameter of the steel tube. The experimental investigation revealed that the torsional capacity of the HC-FCS column significantly depends on the friction exerted between the steel tube and concrete shell and concrete footing. Furthermore, the HC-FCS column had undergone higher rotational drift compared to the corresponding reinforced concrete column.

ACKNOWLEDGMENTS

I would like to express my deep gratitude and sincere thanks to my advisor, Dr. Mohamed ElGawady for his guidance and support during this project and my coursework. It was privilege for working on such an innovative and interesting project under Dr. Mohamed ElGawady. I would also thank Dr. K. Chandrashekhara and Dr. Grace Yan for serving as my advisory committee.

I would specially like to thank my fellow researcher, Omar I. Abdelkarim for guiding me all the time. I would also thank my research team Mohanad Abdulazeez, Ahmed Gheni, Song Wang, and Ayman Moustafa for helping me in the research. I would like to thank High-Bay structural lab staff Gary Abbot, John Bullock, Brian Swift, and Greg Leckrone for their kind assistance throughout the research.

Special thanks to the National University Transportation Center (NUTC) at Missouri University of Science and Technology for funding this research. The kind contribution from ATLAS Tube is appreciated. Discounts on FRP tubes from Grace Composites and FRP Bridge Drain Pipe are also appreciated.

Last but not least, I would like to thank my family. To my parents, Sri Hari Rao and Sridevi, who has encouraged and supported me all the time.

TABLE OF CONTENTS

LIST OF ILLUSTRATIONS

Page

PAPER II

LIST OF TABLES

Page

PAPER I

PAPER II

1. INTRODUCTION

1.1. BACKGROUND

A significant amount of research has focused on developing seismic resistant structures and accelerating construction in a cost-effective manner that reduces on-site construction time, improves work-zone safety, and reduces traffic disruptions. Pre-fabricated bridge systems and bridge moment technique have recently been used to achieve accelerated construction in bridges.

The current research presents innovative hollow-core composite columns namely Hollow-Core Steel-Concrete-Steel (HC-SCS) (Figure. 1.1a) and Hollow-Core Fiber Reinforced Polymer-Concrete-Steel (HC-FCS) (Figure. 1.1b). The HC-SCS column consists of sandwiched concrete shell between the two steel tubes. However for the HC-FCS column, outer steel tube was replaced by the FRP tube. Both columns have numerous advantages over conventional reinforced concrete columns. The new columns were lighter in weight due to reduction in amount of concrete core around 60% to 75%. The HC-SCS and HC-FCS columns generate ease in pre-cast construction which accelerates construction. No additional reinforcements were provided to the columns. Steel tube acts as both longitudinal and transverse reinforcement to the column. Both the inner and outer tubes act as permanent form-work and provide confinement to the concrete. The concrete shell was continuously protected from hast environments due the presence of the outer tube. The inner steel tube was protected from corrosion by the concrete shell and outer tube in both HC-SCS and HC-FCS column. The current research investigates the torsion behavior of HC-SCS and HC-FCS column.

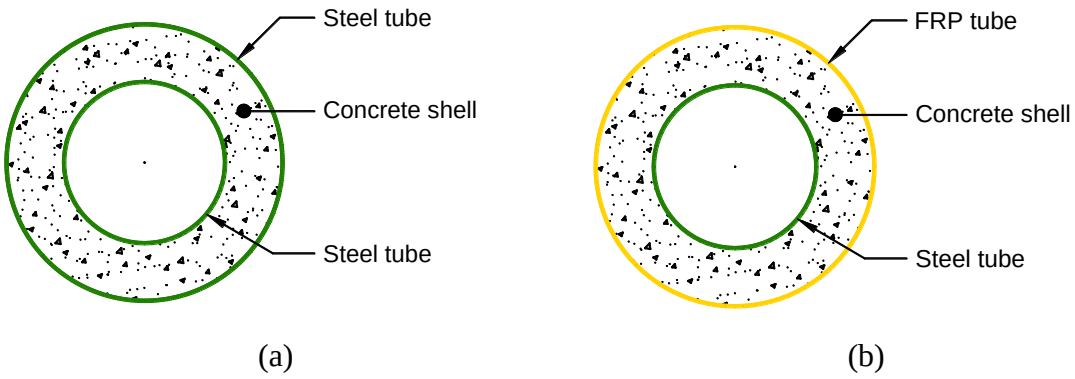

(a) (b)

Figure 1.1. Cross-section (a) HC-SCS column, (b) HC-FCS column

1.2. OBJECTIVES

This research study was conducted in an attempt to understand the behavior of HC-SCS and HC-FCS columns under pure torsion loads. The research on pure torsional behavior of HC-SCS column was limited. Moreover, no previous research was focused on pure torsional behavior of HC-FCS column. The research was divided into two parts.

For the first part, FE models will be developed for HC-SCS column using LS-Dyna and simulated under pure torsion loading. The behavior of FE results will be validated with the experimental results of Huang et al. 2013. Parametric analysis will be performed to better understand the influence of each parameter affecting the HC-SCS column's torsion behavior. Simplified equations will be developed to predict the columns torque capacity.

For the second part, a large scale HC-FCS column was to be constructed and investigated under constant axial load and cyclic pure torsional load. The design criteria and experimental detailing will be proposed. The surface interactions between the steel tube, concrete shell, and FRP tube will be studied.

1.3. THESIS ORGANIZATION

This thesis was organized into three sections. In section 1, the background of composite columns and previous studies were discussed. It also includes the objective of the thesis.

In section 2, a journal paper on torsion behavior of hollow-core steel-concrete-steel (HC-SCS) columns was discussed. A FE model was developed using LS-Dyna and simulated under torsion loads. The FE results were validated with the experimental results of Huang et al. (2013). Parametric analysis was performed by varying strengths of steel tubes and concrete shell, diameter-to-thickness ratio of the steel tubes, concrete shell thickness, and aspect ratio of the column to better understand the torsion behavior of the HC-SCS column. A simplified equation was proposed to predict the column's torque capacity.

In section 3, a journal paper on the torsion behavior of hollow-core FRP-concrete-steel (HC-FCS) column was discussed. The column description and design criteria were discussed. The test setup and loading criteria were discussed. The experimental results were detailed and the comparison was made with the conventional reinforced concrete column in terms of ductility.

2. LITERATURE REVIEW

2.1. CONCRETE-FILLED TUBE COLUMNS

The transformation of the reinforced concrete column to a composite column starts with concrete-filled tubes. The concrete-filled tubes consisted of concrete encased either in a steel tube or a FRP tube. However, the weight of the structure was not decreased compared to the reinforced concrete columns, but the reinforcement detailing was minimized.

2.1.1. Concrete-Filled Steel Tubes. The transformation of reinforced concrete columns to composite columns starts with concrete-filled steel tubes. The steel tube acts as a permanent formwork and provides longitudinal and transverse reinforcement to the column. The column's cross-section shape depends on the applied loads and aesthetics. The circular sections perform better than square section under seismic loads. The confinement provided by the circular section is better than the square section (Xiao and Zhang (2008)). The columns have been widely used in high-raised structures and multi-storey buildings.

The steel tube buckling behavior was either avoided or delayed due to the lateral stability provided by the concrete core. The spalling of the concrete core was avoided and performance was enhanced due to the confinement provided by the steel tube. In concrete-filled steel tubes, the concrete core performs better under axial loads while the steel tube performs better under bending loads. The combination of a steel tube and concrete core enhances the strength and ductility of the column. The concrete-filled steel tubular column exhibits poor fire resistance and corrosion resistance.

2.1.2. Concrete-Filled FRP Tubes. The corrosion of the steel reinforcement in reinforced concrete columns and the steel tube in concrete-filled steel tube was the main reason for the weakening of the columns. An alternate of using fiber reinforced polymer (FRP) in place of steel had gained importance. A new column concrete-filled FRP tube (Mirmiran and Shahawy (1996)) had gained importance. The proximity of fiber direction close to the hoop direction enhanced the confinement to the concrete core, especially under axial loadings. The improved confinement enhanced the strength and ductility of the column. Thus the combination of two brittle members (FRP, steel) provides a ductile member. The use of fiber in place of steel decreases the weight of the column.

Several researchers (Mirmiran and Shahawy 1996; Zhang et al. 2000; Rousakis 2001; Fam and Rizkalla 2001; Lam and Teng 2004; Xiao 2004; Shao et al. 2006; Ozbakkaloglu and Oehlers 2008; Yu and Teng 2010; Abbasnia et al. 2013; Bai et al. 2013) had investigated the static and cyclic behavior of the concrete-filled FRP tube under axial and/or bending loads. The studies show the significant improvement in the concrete core's confinement and the increase in strength and ductility.

2.2. HOLLOW-CORE COLUMNS

The lateral stiffness was the governing factor in designing bridge columns in seismic regions. The core of the column doesn't govern in the lateral stiffness. The hollow-core columns possess several benefits over solid columns. The inertial forces produced during seismic excitations are reduced by decreasing the self-weight of the column. The required amount of longitudinal reinforcement can be significantly decreased for hollow-core column. The investigation of hollow-core reinforced columns

starts with the two layers of longitudinal and transverse reinforcement located at in and out faces of the column with cross ties placed in the concrete shell thickness (Mander et al. 1983). Zahn et al. (1990) investigated the seismic behavior of hollow-core reinforced concrete column with one layer of longitudinal and transverse reinforcement located near the outer face of the column. The investigation revealed that the ductility levels are relatively low compared to two layers of reinforcement.

2.2.1. Hollow-Core Steel-Concrete-Steel Columns. Montage et al. (1978) developed a hollow-core composite column by using concrete shell and steel tube. The HC-SCS consists of concrete shell sandwiched between the two steel tubes. The HC-SCS columns possess excellent benefits over concrete filled tubular columns. The HC-SCS columns were lighter in weight, high stability in local buckling and good cyclic performance.

Several researchers (Wei et al. 1995; Lin and Tsai 2002; Zhao et al. 2002; Tao et al. 2004; Tao and Han 2006; Zhao and Han 2006; Lu et al. 2010; Dong et al. 2012; Hassanein et al. 2013; Li et al. 2014) had investigated the HC-SCS columns under static/cyclic axial and/or bending loads. Under static loadings, the behavior of outer steel tube in HC-SCS was similar to the steel tube in concrete-filled steel tube. The large increase in ductility and energy absorption was observed in HC-SCS columns compared to concrete-filled steel tubes. The difference in Poisson's ratio of steel and concrete had significantly influenced the structural behavior of the HC-SCS column under axial loading. The influence of inner steel tube on the column behavior increases with the diameter of the steel tube. The confined concrete had same behavior in HC-SCS and concrete-filled steel tubes if the ratio of diameter of inner steel tube to concrete shell

outer diameter does not exceed 0.8. No slip was observed between steel tubes and concrete shell.

The HC-SCS columns under contact axial load and cyclic flexure load showed significant increase in strength, ductility, and energy dissipation. The investigator reported that the outer steel tube with circular shape exhibits good ductility and energy dissipation compared to square shape. The design equations proposed by Han et al. (2009) to calculation of HC-SCS columns flexural capacity were good in correlation with the experimental results. The deformation of HC-SCS was relatively faster that concrete-filled steel tubes for a certain time under long-term loading. The ultimate strength of the HC-SCS column decreases with the long term loading and effects were similar to concrete-filled steel tubes.

2.2.2. Hollow-Core FRP-Concrete-Steel Columns. The outer steel tube of HC-SCS column was replaced by FRP tube known as HC-FCS proposed by Teng et al. 2004. The inner steel tube was may be located concentrically center for columns or at an eccentricity (e) for the beams (Figure. 2.1). The corrosive resistance was improved by using FRP in place of steel since; the inner steel tube was protected by the FRP tube and concrete shell. Due to excellent corrosion resistance, the HC-FCS columns were suitable for costal and marine structures which were likely to be exposed under harsh environment. The hoop direction of fiber endeavors the shear capacity of the column and increases the strength and ductility.

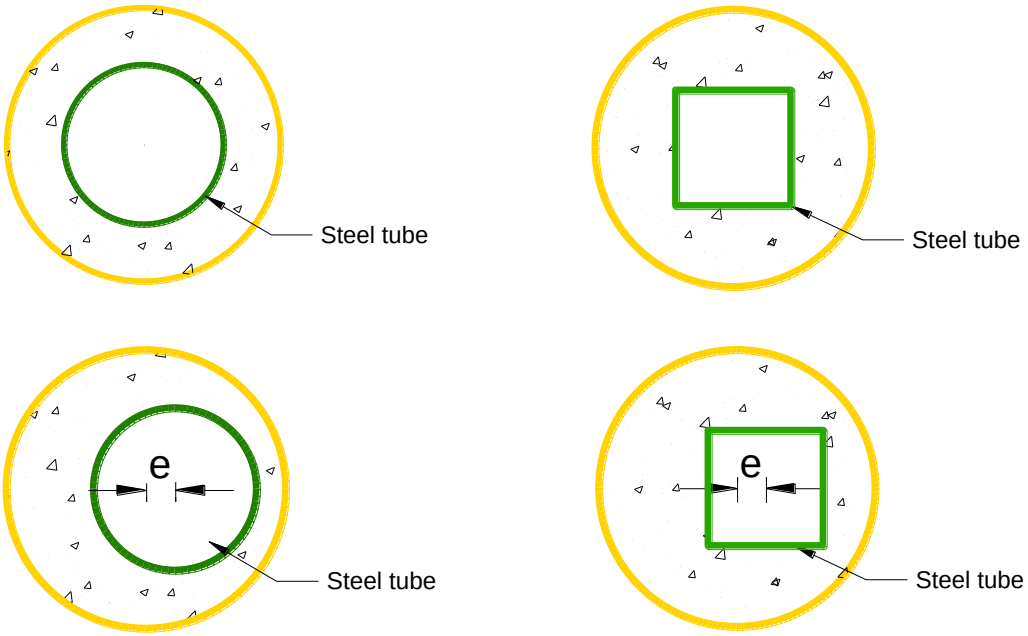

Figure 2.1. Column Cross-section with Different Shape and Eccentricity

Yu et al. (2007), (2010), (2012); Teng et al. (2007); Qian and Liu (2008); Zhang et al. (2011); Ozabakkaloglu et al. (2013); and Abdelkarim and ElGawady (2014a) have studied the behavior of small scale HC-FCS column under monotonic/cyclic axial loads. The investigations revealed that the confinement to the concrete core was improved by the FRP tube and steel tube. The local buckling of steel tube was delayed or avoided by lateral stability provided by the concrete core. The presence of inner steel tube with void decreases the beneficiaries of the outer FRP tube however the loss in confinement to the concrete core from outer FRP tube was compensated by the inner steel tube. Xie et al. 2011 experimentally investigated the large scale HC-FCS columns under monotonic axial loads and confirmed the ductile response of the column. The investigations also revealed

that the concrete shell with outer FRP tube as circular section was better confined than the square section.

Qian and Liu (2008), Han et al. (2010), and Ozabakkaloglu and Idris (2014) had investigated the flexural behavior of HC-FCS columns along with constant axial load. The investigations revealed that the fiber orientation in hoop direction possess high strength compared to the multi-direction. The HC-FCS columns with high strength concrete possess good ductility and seismic response. The increase in FRP layers increases the moment capacity and ductility of the column. The plastic hinge of the column was located at the end of the column within the diameter range of the column. The influence of axial load level has significant effect on the moment capacity and ductility of the column. Addelkarim and ElGawady (2014b) developed a Finite Element model that was in good correlation with the experimental results. Recently Abdelkarim et al. 2015 tested a large scale under constant axial load with cyclic lateral load and concluded the HC-FCS column possess high stiffness and undergo high lateral drift compared to the reinforced concrete columns.

2.2.3. Torsion Significance in Columns and Previous Studies on Composite Columns. During seismic excitations, the bridge columns undergo significant torsion loads along with axial and flexure loads (Figure 2.2). The torsion loads would be significant in skewed or curved bridges, bridges with unequal spans, bridges with outrigger beams, and spandrel beams. In skewed bridges, the collision between bridge deck and abutment cause in-plane rotation of the structure resulting in torsion loads (Tirasit and Kawashima (2005)). The bridges with outrigger bends may undergo torsion loads due to eccentricity of load action. The topography conditions and soil conditions

result in unavoidable construction of such bridges. There is no practical existence of pure torsion loads on the structures. However, the study on pure torsion helps to better understand the column under combined loads including torsion. The detailed investigation of pure torsion studies on composite columns were explained below.

Beck et al. 2003 was first to experimentally investigate the pure torsional behavior of concrete-filled steel tubes. The investigation includes a total of eight columns including concrete column, steel columns, and concrete-filled steel tubes. The post peak response of concrete-filled steel tubes exhibited good ductility and twist compared to steel columns. The concrete column failed abruptly soon it reaches the capacity. The steel columns failed due to local buckling whereas it was avoided in the concrete-filled steel tubes. The crack pattern on the concrete shows 45° with the longitudinal axis. A finite element model was developed using SOLVIA to understand the torsion behavior. A theoretical model was developed with simple equations and predicted the column's ultimate torque.

Han et al. 2007 developed a FE model to investigate the torsion behavior of concrete-filled steel tubes with different cross-sections (circular, square). The investigation revealed the confinement to the concrete core was better provided from circular steel tube than the square steel tube. The concrete core plays an important role in the torsional resistance to the column by providing lateral stability to the steel tubes. The FE model simulations were good in correlation with the experimental results of Beck et al. 2003. The theoretical model developed predicted columns ultimate torque with greater accuracy.

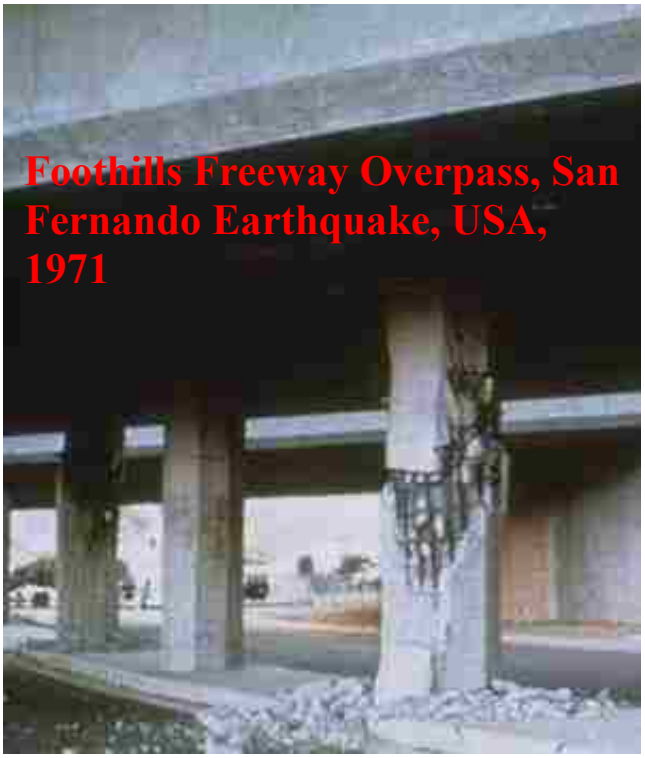

Damage in Buildings due to Kagoshima-ken Hokuseibu Earthquake, 1997

Figure 2.2. Torsion Failure on Columns

Lee et al. 2009 developed a constitutive equation to predict the torsion behavior of the concrete-filled steel tube with confinement effect. The steel tube after yielding exhibited significant plastic deformation without strength deterioration because local bucking of steel tube was avoided by concrete core. The concrete core starts to crack at 45° after the shear strength of concrete reaches its ultimate tensile strength.

Several researchers (Lee et al. 1991; Xu et al. 1991; Nie et al. 2012) investigated the torsional behavior of concrete-filled steel tubes under static/cyclic combined loads. The test results from Lee et al. (1991) revealed the torsional resistance of the concrete-filled steel tubes increases with the applied axial load. However, in contrast, Xu et al. (1991) test results reported that the torsional resistance decreases with the applied axial

load. The researcher also reported that the column height with 20 times the column diameter undergoes higher twist compared to column height with 7 times diameter of the column. The FE models developed by Han et al. (2007) good behavior with the experimental results of Lee et al. 1991, Xu et al. (1991) and lead to development of design equations to predict the columns ultimate torque. Nie et al 2012, 2013 studied the cyclic torsion behavior of concrete-filled steel tubes under combined loadings. The investigator reported that the column's ultimate torque increases with low axial compression and decreases with high axial compression. The stiffness degradation was gradual and exhibited good ductility.

Huang et al. 2013 was first to experimentally investigate the pure torsional behavior of HC-SCS columns. The investigation includes a total of 12 columns with outer steel tube in circular and square shape. The infill of concrete shell between the steel tubes endeavors 20% of the column's ultimate torque. The increase in column's ultimate torque with infill of concrete shell was higher for circular section than square section. The rotational twist of the circular sections was higher than the square sections. No sliding occurred between the concrete shell and the steel tubes. The cracks were occurred at 45° at the middle height of the concrete shell. Design equations were proposed based on the FE model results to predict the column's ultimate torque. Both the FE and designed equation results were good in correlation with the experimental results.

PAPER

I. BEHAVIOR OF HOLLOW-CORE STEEL-CONCRETE-STEEL COLUMNS SUBJECTED TO TORSION LOADING

Sujith Anumolu[1], S.M. ASCE; Omar I. Abdelkarim[2], S.M. ASCE; Mohamed A. ElGawady[3§], PhD, M. ASCE

Abstract

This paper presents the torsional behavior of hollow-core steel-concrete-steel (HC-SCS) columns using finite element (FE) and analytical approaches. HC-SCS column consists of a concrete shell sandwiched between two steel tubes. Ls-Dyna software was used to develop a three-dimensional HC-SCS model and simulated under torsional loading. FE results were validated against the experimental results collected from six HC-SCS columns tested under pure torsion. The average error from FE analysis was 4.8% compared to experimental results, when predicting the column's torsion strength. The study revealed that the interaction between the steel tube's stiffness and concrete shell's thickness controls the behavior of the column. A parametric study was conducted for further analysis of each parameter that was affecting the column's torsion behavior. The parametric analysis concluded the torsional behavior of the column mainly depends on the outer steel tube's properties and thickness of the concrete shell. A simplified equation was developed to predict the torsion strength of the member using direct method of stress

1 Graduate Research Assistant, Dept. of Civil, Architectural, and Environmental Engineering, Missouri University of Science and Technology, Rolla, MO. 65401; sat6f@mst.edu
2 Ph.D. Candidate, Dept. of Civil, Architectural, and Environmental Engineering, Missouri University of Science and Technology, Rolla, MO. 65401; oiafgc@mail.mst.edu
3 Benavides Associate Professor, Dept. of Civil, Architectural, and Environmental Engineering, Missouri University of Science and Technology, Rolla, MO. 65401; elgawadym@mst.edu
§Corresponding author

analysis. The proposed equation predicted the members' torsional strength with accuracy more than 90%.

Introduction

Researchers have recently focused on developing new cost-effective design and construction methods for accelerating bridge construction (ABC) which leads to improved site constructability and work zone safety as well as reduction in traffic disruptions and life-cycle costs (Dawood et al. 2012; Abdelkarim et al. 2015a). One approach to accelerate bridge columns and shafts construction, while obtaining higher seismic performance is to use concrete-filled steel tubular (CFST) columns in which concrete core is encased in steel tube.

CFST members possess several benefits over reinforced concrete (RC) or steel members. The steel tube in CFST acts as stay-in-place formwork, longitudinal and shear reinforcements to the member, and continuous confinement to the concrete core. Furthermore, the concrete core in CFST acts as bracing to the steel tube providing lateral stability which delays steel tube local buckling. Hence, CFST displayed superior performance under earthquake ground motions (Bi et al. 2013).

A typical bridge column would sustain 5% to 10% of its ultimate axial load capacity due to service axial loads (Mondal and Prakash 2015a). Design of bridge columns in seismic regions are typically controlled by bridge lateral stiffness demand. Hence, researchers developed hollow-core CFST system. The system consisted of an inner steel tube and outer steel tube and concrete filled between the two tubes (Wei et al. 1995; Lin and Tsai 2001; Zhao et al. 2002; Tao and Han 2006). The main advantage of hollow-core

steel-concrete-steel (HC-SCS) columns is the high strength to weight ratio compared to columns having solid cross sections. Lighter weight is crucial for precast construction to reduce freight cost. Furthermore, reducing the columns weight will reduce the seismic inertial forces in the case of long columns.

A number of investigators recently studied the behavior of HC-SCS columns under different type of loading conditions (Yagishita et al. 2000; Zhao et al. 2010; Elchalakani et al. 2002; Tao et al. 2004; Han et al. 2006; Lu et al. 2010; Dong and Ho 2012; Hassanein et al. 2013; Li et al. 2014). Most of the studies were limited to axial and flexural loadings with different cross-sections. These studies depicted that the action of confinement was active after the concrete shell cracks and dilates. In addition, they reported that the buckling of the steel tubes was significantly delayed due to the lateral support from concrete. Also, they found that the influence of concrete shell thickness on the ductility of the column was small.

Bridge columns are subjected to torsional loads in curved and skewed bridges during the earthquakes. Typically, torsion exists in a combination with axial and flexural loads. However, since torsional behavior is complicated, most of researchers investigated the performance of bridge columns under pure torsional loads to better understand columns behavior (Beck and Kiyomiya 1996; Han et al. 2007; Lee et al. 2009; Nie et al. 2012; Huang et al. 2013). Other researchers investigated the behavior of bridge columns under combined torsional, flexural, and/or axial loads (Lee et al. 1991; Xu et al. 1991; Belarbi et al. 2008; Prakash and Belarbi 2009; Mullapudi and Ayoub 2012; Ruili et al. 2014; Mondal and Prakash 2015a,b). Most of these torsional studies were on conventional reinforced concrete columns or CFSTs. However, very few researches were conducted to

study the torsional behavior of HC-SCS columns. Under pure torsion, the RC columns failed due to spalling of concrete and rupture of transverse reinforcement at the middle height of the column. However, the concrete spalling was avoided due to confinement of steel tubes in HC-SCS columns. The confinement of steel tubes endeavors the torsional load carried by the concrete shell.

Huang et al. (2013) was the first to experimentally investigate the pure torsional behavior of HC-SCS columns. The investigation of HC-SCS columns has shown significant strength, ductility, and energy absorption. The investigation revealed the presence of concrete shell enhanced 20% of the column's torsion capacity. The researchers reported that the concrete shell cracks at 45 º to the axis and maintained its shape. The concrete shell was well bonded with the outer steel tube as no sliding was observed. They reported that the outer steel tube's strength and thickness were important parameters affecting the torsion behavior..

This study investigates the torsional behavior of HC-SCS columns using 3D finite element (FE) analysis. The FE models were validated with experimental results of six HC-SCS columns recently tested by Huang et al. (2013). The validated FE models were used to analyze and better understand the behavior of HC-SCS columns under pure torsion. An extensive parametric study was conducted to investigate important parameters affect the torsional behavior of the HC-SCS columns. The parametric study included wider ranges of diameter-to-thickness ratios of both steel tubes, yield strength of the outer and inner steel tubes, the cylindrical unconfined compressive strength of the concrete (f_c'), existence of concrete shell or inner steel tube, height-to-diameter ratio of

the column, and concrete shell thickness. Furthermore, this paper proposes simple design equations to calculate the torsional strength of HC-SCS column.

FE Modeling

Geometry

A total of six columns, namely CO111, CO112, CO211, CO212, CO311, and CO312 were tested by Huang et al. (2013). Each column had a height (H) of 550 mm (21.6 in.) and an outer steel tube's diameter (D) of 165 mm (6.5 in.) (Figs. 1 and 2). The thickness of the outer steel tube (t_o) varied from 3.0 mm to 4.6 mm (0.12 in. to 0.18 in). The inner steel tube's diameter (d) was either 42 mm (1.7 in.) or 75 mm (2.9 in.) with thickness (t_i) varied from 3.0 mm to 5.0 mm (0.12 in. to 0.20 in.). Hence, the concrete shell thickness ranged from 40.4 mm to 58.5 mm (1.60 in. to 2.30 in.). Two steel plates having dimensions of 235 mm x 235 mm x 25 mm (9.25 in. x 9.25 in. x 0.98 in.) were attached to the column's top and bottom surfaces. The bottom steel plate of each column was fixed to the column from one side and to the ground from the other side. The top plate was connected to the column from one surface and to a loading plate from the other surface. The loading plate was 94 mm x 324 mm x 25 mm (3.7 in. x 12.76 in. x 0.98 in.; Fig. 1). Hence, the specimens examined in this study were tested as cantilever columns under pure torsion with fixation of columns to their footings. All of the columns were symmetric around the X and Y axes and the rotational displacement was applied using the loading plate around the Z-axis. Table 1 summarizes the columns' variables.

A sensitivity analysis was performed to identify the elements' dimensions that result in a good balance between accuracy of the solution and solution time. Each column's

concrete core, steel top and bottom plates, and loading plate were modeled using 8-node brick solid elements. The concrete element's size had an average size of 8.75 mm x 15 mm x 10 mm (0.3 in. x 0.6 in. x 0.4 in.). The element's size of steel plates and loading plate had an average size of 23.5 mm x 23.5 mm x 12.5 mm (0.9 in. x 0.9 in. x 0.5 in.). Steel tubes were simulated using 4-node shell elements. A typical element's size of the outer steel tube was 21.6 mm x 10 mm (0.8 in. x 0.4 in.). The typical element's size of an inner steel tube was 7.8 mm x 10 mm (0.3 in. x 0.4 in.). Each FE model had 11,072 elements and 13,047 nodes.

To reduce the analysis time, all the solid elements of the column were modelled with constant stress and one-point quadrature integration. An Hourglass control was used to avoid spurious singular modes of the elements. The hourglass value for all of the models was considered as the default value of 0.10 (Abdelkarim and ElGawady 2014(b)).

Material Models

Concrete

Various material models are available in Ls-Dyna to simulate the concrete material. The Karagozian and Case Concrete Damage Model Release 3 (K&C model) was used in the current study since it was used by several researchers for similar applications and resulted in good predictions of the performance of the investigated elements (e.g. Abdelkarim and ElGawady 2014b and 2015b, Ryu et al. 2014, Youssf et al. 2014). The model is built on the theory of plasticity with three shear failure surfaces: yield, maximum, and residual (Malvar et al. 1997).

The concrete cylindrical compressive strength f_c' was 42 MPa (6,090 psi) for all of the columns. In K&C model, the yield and failure surfaces' parameters are automatically

generated with the input of f_c'. A default value of 0.5 was used for fractional dilation parameter (ω) that considers the volumetric change in concrete. The compressive behavior of the concrete shell under tri-axial stresses was controlled by equation of state (EOS) that was automatically generated using the Eq. (1) (Noble et al. 2005, Crawford and Malvar 2006). The tri-axial stress state for the concrete shell was achieved only at the contact surfaces between the concrete shell and steel tube. The micro cracking of the concrete shell was delayed due to the confinement provided from the steel tubes

$$K = \frac{E_c}{3(1-2\upsilon)} \quad (1)$$

where υ is Poisson's ratio, and E_c is the elastic modulus, taken as 0.2 and 57000 $\sqrt{f_c'}$ (ACI-318 (2014**)**) in this study, respectively.

Under the axial tension, the concrete cracks were distributed throughout the height of the HC-SCS column rather than brittle failure for a plain concrete at the middle height of the column. Moreover, the crack with in the HC-SCS column was limited due to the bond stress developed between the steel tubes and the concrete shell (Lee et al. 2014).

Steel Tube

An elasto-plastic material model "003-plastic_kinematic" was used to describe the steel tube's stress-strain curve. The main parameters that were needed to describe this material model are the yield stress (f_y), elastic modulus (E), and Poisson's ratio (ν). For all of the models in this manuscript, f_y varied from 260 MPa (37,710 psi) to 365.4 MPa (52,997 psi), E was taken as 200 GPa (29,000, ksi), ν was taken 0.3. The steel tubes ultimate strain was considered as 0.04 (Abdelkarim and ElGawady 2014a). Once a steel element ruptured either in shear or axial tension, it was removed from the model using erosion

feature in Ls-Dyna to ensure the mode of failure. Under torsion loadings shear forces were exerted. The shear forces were in diagonal direction and resolved into resultant force in horizontal and vertical direction. The vertical force induces axial tension in the column. So add erosion parameter was studied to ensure the failure mode.

Steel Plates and Loading Plate

During the experimental work, no damage was observed in any of the top, bottom, and loading plates; hence, all three plates were models using linear elastic material model. This material model was defined using a value of 200 GPa (29,000 ksi) for the steel elastic modulus (E) and 0.3 for the Poisson's ratio.

Concrete-Steel Interfaces

The steel tube and concrete shell surfaces are interfaced by surface-to-surface contact element simulation which allows slip and separation between the two materials. The friction coefficient between the steel tubes and the concrete shell was considered as 0.6 (Rabbat and Russel 1985; Abdelkarim and ElGawady 2014b). The steel tubes were fixed to the top and bottom steel plates during the experimental work. Hence, tied node-to-surface contact elements were used to bond the top and bottom steel plates to the column's top and bottom surfaces to simulate the full fixation during the experimental work. For the same reason, the loading plate was fully contacted to the top surface of the top steel plate using tied surface-to-surface contact elements. The concrete shell and steel plates were contacted by node-to-surface contact. Based on the sensitive analysis and from the previous studies, the friction coefficient of 0.6 (Abdelkarim and ElGawady 2014b) was assumed between the contacts. Since the concrete was enclosed between two

steel tubes which resist the loss of moisture from the concrete. The shrinkage affects were minimal and can be neglected.

Loading and Boundary Conditions

The displacements and rotations degrees of freedom were restrained at the bottom of the steel plate to simulate fixation similar to what was used during the experimental work. The top of the loading plate was directionally restrained in the Z-direction to simulate the restraint from the hydraulic jacks used during the experiment. During the experimental work, the torque was applied through applied at two equal magnitude displacements in opposite directions at the ends of the top loading plate with an arm length of 278 mm (2.3 in.) as shown in Fig.1. The torque was applied to the column until the jack reached its maximum travel stroke. The experimental work was truncated before the failure of the columns due to limit in rotational limit of the jacks. Similar loading procedure was used during the finite element. However, the columns in FE were subjected to the torque until the columns failed in the form of either steel tube rupture or concrete shell failure.

Results and Discussion

Huang et al. (2013) defined the torque corresponding to a maximum shear strain in the outer steel tube of 0.01 ($\gamma_{os,0.01}$) as the torsional strength ($T_{FE,\ 0.01}$) of the investigated columns. Beyond that shear strain, the increase in the torsion moment is quite small and can be ignored for practical applications (Huang et al. 2013). Table 2 summarizes the experimental torsional strength (T_{ue}) reported by Huang et al. (2013). The torsion strength obtained using the FE at $\gamma_{os,0.01}$ ($T_{FE,\ 0.01}$) is also presented in Table 2.

Furthermore, Fig. 3 shows the torque - twist relation of all of the columns for the experimental and FE results. The twist was calculated at the top of the column.

As shown in the table and figure the values of T_{ue} and $T_{FE,0.01}$ were in a good agreement with the FE. The FE over-predicted the strength of four columns while under-predicted the strength of two columns. The error values ranged from 1.3% to 10.2% where the error values were calculated as the absolute value of the difference between the experimental and the FE results divided by the experimental results. Furthermore, the model was able to predict the twist at $\gamma_{os,0.01}$ in within an average error of 10%.

General Behavior of the Columns

As shown in Fig. 3, all the columns behaved very similar with elasto-plastic behavior. This section will detailed the performance of column CO111 and then briefly report the results of the other columns. Before yielding of the outer steel tube which occurred at a twist of approximately 1º, the relationship between the torque and twist displayed slight gradual stiffness degradation and the relationship can be considered approximately linear. The stiffness degradation occurred when some of the concrete shell elements went beyond their ultimate tensile capacity leading to gradual stiffness degradation in the models.

Typical shear stress - shear strain relation of two concrete elements at the middle height section where failure occurred is shown in Fig. 4. The diagonal cracks occurred in the concrete shell induces compressive strain on the concrete elements along the crack and the surrounding region experiences tensile strains. In the Fig. 4, one of the concrete elements was subjected to tensile strains and the other concrete element was subjected to compressive strains. As shown in the Fig.4 once the outer steel tube yielded, more shear

strain demand imposed on the concrete shell leading to excessive principle tensile stresses. Beyond shear strain value of 0.002 corresponding to a twist of 0.75° the concrete element reached to zero stiffness.

Column CO111 reached $T_{FE,0.01}$ of 26.0 kN.m (19.2 kip.ft.) during the FE analysis and 24.6 kN.m (18.1 kip.ft.) during the experimental work (Fig. 3a). The FE over-estimated the strength of the column by 5.4%. The twist of the column at 0.01 shear strain in steel was 2.7° for both the experimental work and FE analysis (Fig. 3a).

While the experimental work terminated when at $\gamma_{os,0.01}$, the FE analysis was able to continue beyond this strain value. Fig. 6 shows the backbone curves for this set of columns until failure occurred. As shown in the figure, beyond $\gamma_{os,0.01}$, the twist at the top of the column increased considerably with limited increase in the torsion capacity. The increase in the torsion capacity ranged from 17% to 28% compared to the $T_{FE,\ 0.01}$ while the twist increased by approximately 9.0 to 15.0 times the twist at 0.01 shear strain in steel. . Beyond $\gamma_{os,0.01}$, the FE models showed that the concrete shell displayed significant cracking and expansion in volume. The yielding of outer steel tube resulted in loss of confinement to the concrete shell from outer direction. However, the existence of the inner steel tube constrains the concrete from expanding its volume in inner direction and decrease damage in the concrete shell. The expansion in volume of concrete shell was not effective in inner direction compared to outer direction resulted small increase in damaged concrete strength. The concrete starts to crack after it reaches poisson's ratio of 0.2 and starts to expand its volume. The volume expansion of concrete was countered by the steel tubes from both inner and outer direction. Fig. 4(a) shows the increase in the concrete compressive strength beyond γ of 0.014. Table 3 summarizes the shear stress of

the outer steel tube at rupture and torsion capacity carried by the FE columns. The shear stress at failure was considered from the outer steel tube because it failed first.

By increasing the applied torque beyond the yielding of the outer steel tube, significant stiffness softening occurred leading to significant increase in the twist with minimal increase in the applied torque. This led to yielding of the inner steel tube at a twist ranged from 2° to 3°.

Fig. 5 shows a typical relationship between the shear stress versus shear strain, and shear stress versus twist for elements of the concrete, inner steel tube, and outer steel tube at the point of failure of the column CO111. As shown in the figure, before yielding of the outer steel tube, the outer steel tube's shear stress was more than triple that of the inner steel tube's shear stress indicting that the torsion strength is mainly provided by the outer steel tube. Furthermore, the inner steel tube's shear stress increased significantly after yielding took place in the outer tube. It should be noted that the inner steel tube yielded at higher stress compared to the outer steel tube since both tubes have a slightly different material characteristics as show in Table 1 and reported by Huang et al. 2013. Once yielded, each tube displayed strain hardening until failure. After the rupture of outer steel tube, the torsion resistance of the column reduced by about 70%. No vertical slip occurred between the concrete shell and steel tubes throughout the column's height due to the constraint imposed by the test setup.

Fig. 7 shows the column's failure mode obtained using the FE model. All of the six columns failed in a similar manner. The failure was triggered by rupture in the outer steel tube in the helical direction at the mid-height of each column. Failure of an element in Ls-Dyna is indicated by removing the element using the erosion option as explained

earlier in this paper. Rupture occurred in several elements at the outer steel tube resulted in loss of confinement for concrete in outward direction; this resulted in an increase of concrete shell's volume in outward direction which caused the failure of concrete shell. Finally, the inner steel tube alone carried the applied torque for a small imposed rotation after the concrete shell failed leading to abrupt rupture of the inner steel tube. The failure of inner steel tube was abrupt due to absence of concrete shell that provided lateral stability. The outer steel tube ruptured in the helical direction at 390 mm (15.4 in) from the column's bottom. The shear stress of the outer steel tube of the column CO111 at the failure was 191 MPa (27,702 psi). The concrete's maximum shear stress was considered when the initial small portion of concrete elements failed prior to failure of column. The torsion capacity ($T_{FE,\ u}$) carried by the column CO111 before the failure was 33.3 kN.m (24.9 kip.ft.) and has ultimate twist of 43.8°.

The torsion strength and twist of the columns at 0.01 shear strains in the steel during the finite element study was summarized in Table 2 and displayed in Fig. 3. The torsion capacity (T_{FE}, u) for the columns during the finite element study was summarized in Fig. 6. Fig. 8 shows the typical contribution of steel tubes and concrete shell towards the torsion moment and effect of confinement. The columns CO112, CO211, CO212, CO311, and CO312 reached FE torsion strength ($T_{0.01}$) at 34.5 kN.m (25.5 kip.ft), 35.6 kN.m (26.2 kip.ft), 44.3 kN.m (32.6 kip.ft), 47.5 kN.m (35.1 kip.ft), and 53.6 kN.m (39.50 kip.ft) compared to experimental value of 33.2 kN.m (24.5 kip.ft), 32.3 kN.m (23.8 kip.ft), 42.1 kN.m (31.05 kip.ft), 48.8 kN.m (36.00 kip.ft), and 54.3 kN.m (40.0 kip.ft). The torsion capacity (T_{FE}, u) of the FE columns (CO112, CO211, CO212, CO311,

and CO312) was between 41.7 kN.m (30.8 kip.ft) and 63.9 kN.m (47.1 kip.ft). The ultimate twists of these columns were shown in Fig. 6.

Parametric Study

Parametric study was conducted to study the influence of the main parameters of the column including the concrete's strength (f_c'), the outer steel tube's strength (f_{yo}), the inner steel tube's strength (f_{yi}), the outer steel tube diameter-to-thickness ratio (D/t_o), concrete shell thickness (t_c), inner steel tube diameter-to-thickness ratio (d/t_i), and the aspect ratio (H/D) on the torsional performance of HC-SCS columns.

The column CO112 was used as the reference column for this study with both steel tubes chosen to have identical yield strength. Table 4 summarizes the parametric study variables and results. The modes of failure of the investigated columns were similar to those described before. Fig. 9 illustrates the torque-twist relation of all of the investigated columns of the parametric study. Fig. 10 illustrates the percentage change in the torsion capacity of the HC-SCS column with respect to the change in parameters.

Yield Strength of Outer Steel Tube (F_{yo})

The outer steel tube's yield strength ranged from 310 MPa to 586 MPa and ultimate strain was maintained constant for all columns. Expectedly, the column's torsion capacity linearly increased (Fig. 10a) as the outer steel tube's yield strength increased, since failures of these columns were triggered by rupture of the outer steel tube (Fig. 9a). The torsion capacity increased by 45% when the yield strength of the outer steel tube increased by 86%. However, the ultimate twist of the column decreased by 13%.

Expectedly, the yield strength of outer steel tube affects the behavior of the inner steel tube. As the yield strength of the outer steel tube increased, the contribution of the inner steel tube to the torsional resistance before the yielding of the outer tube decreased. However, the overall shear stress imposed on the inner steel tube before the failure of the column remained equal for different strengths of the outer steel tube. It indicated the change in torsional strength was significant before the yielding of outer steel tube with change in its yield strength. However, all of the columns behaved in a similar manner after the outer steel tube yielded.

Yield Strength and Role of Inner Steel Tube (F_{yi})

The inner steel tube's strength was varied between 310 and 586 MPa and ultimate strain was maintained constant for all columns (Fig. 9b). The inner steel tube yield strength had small effect on the column's torsion capacity. The column's torsion capacity linearly increased by 16.5% when the inner steel tube's strength increased by 86% (Fig. 10b). The removal of inner steel tube resulted in 13% decrease in column's torsion capacity (Fig. 9b). It indicated that the inner steel tube's existence had moderate effect on the column's torsional behavior. With increase in inner steel tube's strength, the ultimate twist was increased by 3.5%. Before yielding of the outer tube, the stress concentration on outer steel tube was same for all the columns. Beyond yielding of the outer tube, the column with higher inner steel tube's yield strength (ie. 586 MPa) displayed higher stiffness. Since, post yielding of outer steel tube, most the torsional load was carried by inner steel tube. The stress concentration on the concrete shell was almost same for all the columns. This resulted in no change in behavior of the concrete shell with respect to change in inner steel tube's strength.

Strength (f'_c) and Role of Concrete

The concrete strength was varied between 10 MPa and 100 MPa. While the 10 MPa concrete may not be qualified as a candidate for structural applications in many codes and standards, it was used in this parametric study to investigate a wider range of parametric study.

The torsion capacity increased by 18% and the corresponding ultimate twist increased by 4% when the concrete strength increased by 90%. The torque- twist backbone curve was illustrated in Fig. 9c. The backbone curves depicts that the concrete strength had less impact over the torsion capacity compared to ultimate twist. All of the outer steel tubes yielded at the same strain value confirming the individual behavior of steel tubes and concrete shell before yielding of the outer steel tube.

Before yielding of the outer steel tube, there was a significant increase in the stiffness of the column with the increase in concrete strength. It was observed that the increase in torsion capacity was due to initial stiffness of the concrete shell and the lateral stability provided by the concrete shell to the steel tubes. The concrete shell was removed in an additional column to observe the behavior of the column and the contribution of concrete shell in the capacity of the column (Fig. 9c). The column's torsion capacity decreased by 35% (with respect to f'_c = 40 MPA) without the presence of concrete shell. This reduction in torsion capacity occurred because the outer and inner steel tubes were not braced laterally which was the concrete effect. Therefore, the failure was warping in outer steel tube with wall buckling as shown in Fig. 11. As the concrete was brittle in nature, the increase of its strength increased the brittle character of the column as observed in the form of low twist with increase in concrete strength

D/t_o of Outer Steel Tube

The D/t_o of the outer steel tube was varied between 15 and 250 in order to study the stiffness and buckling behavior of the outer steel tube. The change in the D/t_o was achieved by changing the thickness of outer steel tube from 0.66 mm (0.03 in.) to 11mm (0.43 in.). As shown in Fig. 9d, the outer steel tube's D/t_o was one of the most influential parameters. The column's torsion capacity decreased 5.7 times and ultimate twist increased 1.32 times when the outer steel tube's D/t_o increased from 15 to 250 (Fig. 9d). The effects of the change in the stiffness of the outer steel tube due to changing the D/t_o ratio was more prominent before yielding of the outer steel tube as observed in the torque versus twist curve (Fig. 9d). As explained earlier, after yielding in the outer steel tube, strain hardening occurs in the outer steel tube and most of the torsional load was carried mainly by the inner steel tube. Hence, the effect of changing D/t_o after the yielding of the outer tube diminished. It is worth noting that the AISC manual defines the critical local buckling of the empty steel tube was at diameter-to-thickness value of $0.07\left(\frac{E}{f_y}\right)$. This local buckling critical d/t for the investigated column was calculated as 36.8. The FE analyses showed no local buckling in the steel tubes even at a D/t_o value of 250. This was because of the lateral stability provided by the concrete shell to the steel tube.

The shear stress capacity of the concrete shell at failure of the outer steel tube was decreased for the higher D/t_o ratio. This was due to the decrease in confinement to the concrete shell provided by the outer steel tube. However, since the contribution of the concrete shell to the torsion capacity of the columns is relatively limited, this change in the confinement effect did not significantly change the strength of the columns. As mentioned before, local buckling was not observed in any case. Hence, the shear stress

carried by the inner and outer steel tubes at failure remained constant for different D/t_o ratios.

d/t_i of Inner Steel Tube

The d/t_i of the inner steel tube was varied between 15 and 250 in order to study the stiffness and buckling behavior of the inner steel tube. The change in the d/t_i was achieved by changing the thickness of inner steel tube from 0.3 mm (0.01 in.) to 5 mm (0.2 in.). The inner steel tube d/t_i had a little influence on the column's torsion capacity. The column's torsion capacity decreased by 20% and ultimate twist decreased by 7% when d/t_i of the inner steel tube increased 15.6 times (Fig. 9e). Based on the above parametric study, the geometric term associated with the torsion capacity was section modulus. For small diameters of the inner steel tube with respect to the diameter of outer steel tube, the section modulus of inner steel tube was not much varied with alter in d/t_i ratio. It resulted in small change in column's torsion capacity for smaller diameters of inner steel tube. As expected, the stiffness of the column was decreased with the increase in inner steel tube's d/t_i ratio. The behavior of the outer steel tube and the concrete shell were not altered with the inner steel tube's d/t_i ratio. The ultimate twist of the column was not significantly influenced, since the behavior of the column was mainly associated with the outer steel tube. The ultimate twist decreased with increase in inner steel tube's d/t_i ratio. The increase in thickness of the inner steel tube increases the section modulus resulting in increase of torsional rigidity of the columns. The high torsional rigidity imposes low twist on the column.

Concrete Shell Thickness (t_c)

The concrete shell thickness had major contribution to the torsion capacity of the column. The concrete shell thickness was varied from 15 mm (0.6 in) to 60 mm (2.4 in.) representing 9.1% to 36.4% of the column's outer diameter. To maintain constant diameter-to-thickness ratio of the inner steel tube, the thickness of the inner steel tube was varied with change in concrete shell thickness. While the lower end in the investigated parameter may not reflect practical application it was used to obtain a thorough understanding of the effects of the concrete shell on the performance of HC-SCS columns. The column's torsion capacity and ultimate twist decreased by 56% and 12%, respectively with 300% increase in the concrete shell's thickness (Fig. 9f). The significance of inner steel tube towards the torsional load became prominent with change in concrete shell's thickness. The contribution of inner steel tube to the column's torsion capacity decreased with the increase of concrete shell thickness, since the section modulus of inner steel tube was decreased.

At the point of yielding in steel tube, the steel tubes reached yielding almost at the same time for 15 mm (0.6 in) concrete shell thickness whereas, yield strength of inner steel tube was almost half of the yield strength of outer steel tube for 60 mm (2.4 in.) concrete shell's thickness.. It indicated that the increase in concrete shell's thickness delays the yielding of the inner steel tube. This was due to decrease in stress concentration on the inner steel tube with increase in concrete shell's thickness. Moreover, the contribution of inner steel tube towards torsion capacity reduces with increase in concrete shell thickness. Both the steel tubes failed at the same time for smaller concrete shell's thickness (ie. 15 mm (0.125 in.)) while the inner steel tube's

failure was delayed for larger concrete shell's thickness (ie. 60 mm (2.4 in.)). As the concrete was brittle in nature, increase in its thickness resulted in decrease of the ultimate twist as observed in Fig. 9f.

Aspect Ratio of Column (H/D)

The H/D ratio has very small influence on the column's torsion capacity but has high influence on the ultimate twist. The H/D ratio was varied between 2.1 and 5.7. The column's torsion capacity increased by 10% and ultimate twist increased by 210% when the column's aspect ratio increased by 170% (Fig. 9g). From the Fig. 9g, the torsion capacity of the columns remained approximately constant for different H/D ratios since the torsion capacity depends mainly on the material and cross sectional characteristics of the columns. However, after yielding of the outer tubes, the column with higher H/D ratio displayed significant stiffness softening resulting in significant increase of the ultimate twist at failure (Fig. 9g). The column's mode of failure was outer steel tube rupture as in previous parameters. The increase in aspect ratio results in slenderness of the column and becomes less susceptible towards the applied torsional load.

Analytical Model

In this section, a simple analytical model to calculate the torsion capacity of HC-SCS columns is developed and presented. The analytical torsion capacity (T_a) of the HC-SCS columns can be calculated as the sum of three components: capacity of outer steel tube (T_{os}), concrete shell (T_c), and inner steel tube (T_{is}) as per equation (2). The change in diameter-to-thickness ratio and the yield strength of the inner steel tube doesn't endeavor

the column's torsion capacity significantly. Therefore, confinement to the concrete shell was considered only from the outer steel tube whereas neglected from the inner steel tube.

$$T_a = T_{os} + T_c + T_{is} \tag{2}$$

For calculating the torsion strength of the concrete shell, a segment with an area (*dA)* located at a radial distance of 'a' was selected on the top surface of the concrete shell (Fig. 12). The inner and outer radii of concrete shell are 'r', and 'R'. The height of the column is 'H'. The applied torque resulted in a twist of 'θ' and shear strain of 'γ'.

$$\text{The rotated arc length, } dl = a * \theta = H * \gamma \tag{3}$$

$$\text{From Eq. 3, } \gamma = \frac{a*\theta}{H} \tag{4}$$

$$\text{The Hooke's law states } \tau = G * \gamma \tag{5}$$

$$\text{From the Eq. 5, the Eq. 4 transforms to } \tau_x = \frac{G*a*\theta}{H} \tag{6}$$

Where G is the shear modulus, τ_x is the shear stress of the elementary concrete segment

From the Eq. 6, the shear stress has linear relation with the radius of the column (Fig. 12). The elementary shear force (dF) over the segmental area (dA) was calculated as:

$$dF = \tau_x dA \tag{7}$$

The torque capacity of the concrete shell (T_c) was obtained by integrating the elementary shear force (dF) multiplied by lever-arm (a) over the entire cross-sectional area (A) of the concrete shell.

$$T_c = \int_r^R dF * a = \int_r^R (\tau_x dA) a \tag{8}$$

The application of similar triangle rule for the Fig. 12c based on Eq. 6

$$\frac{a}{R} = \tau_x / \tau_{max} \tag{9}$$

Upon substituting the Eq. 6 in the Eq. 5 and over integration,

$$T_c = \frac{\tau_{max}}{\mathrm{R}} J_{pc} \tag{10}$$

Where was sectional modulus of concrete shell, $J_{pc} = \frac{\Pi(R^4 - r^4)}{2}$ (11)

From the manual ACI-318 (2014), the cracking shear strength (τ_{max}) of the concrete

$$\tau_{max} = 4\sqrt{f'_{cc}} \tag{12}$$

The presence of steel tubes provides confinement to the concrete shell that enhances the compressive strength known as confined compressive strength of concrete (f'_{cc}) was calculated from previous studies (Lee et al. 2009).

Similarly, the torsion strengths of the steel tubes (T_{os} and T_{is}) as below:

$$\text{Torsion strength of outer steel tube } (T_{os}) = \tau_{yo} \frac{J_{po}}{R_o} \tag{13}$$

Where, τ_{yo} and J_{po} are shear stress and polar moment of inertia of outer steel tube respectively. R_o was the outer radius of the outer steel tube

$$\text{Torsion strength of inner steel tube } (T_{is}) = \tau_{yi} \frac{J_{pi}}{R_i} \quad (14)$$

Where, τ_{yi} and J_{pi} are shear stress and sectional modulus of inner steel tube, respectively. R_i was the outer radius of the inner steel tube. The relation between the shear strength and yield strength of steel tube was obtained from Tabor (2000).

$$\text{Shear strength of outer steel tube } (\tau_{yo}) = \frac{f_{yo}}{\sqrt{3}} \quad (15)$$

$$\text{Shear strength of inner steel tube } (\tau_{yi}) = \frac{f_{yi}}{\sqrt{3}} \quad (16)$$

The applied torque resulted in a twist (θ: Fig. 12), where θ can be calculated using Eq. 17 based on Eq. 6.

$$\theta = \frac{(T_a * H)}{(G * J)} \quad (17)$$

The analytical model's results were compared to the experimental results in Table 2 and Fig. 3. The analytical model had an average error of 9.4% with the experimental value in predicting column's torsion strength. The parametric results of FE and the analytical model are good in agreement (Table 4). The torsion capacity of the inner steel tube will become effective with increase in its section modulus.

Summary and Conclusions

The Ls-Dyna software was used to conduct a finite element analysis of hollow-core steel-concrete-steel columns (HC-SCSs). The HC-SCS consisted of a concrete wall that was sandwiched between steel tubes. The finite element analysis results were validated against experimental results available in the literature. The proposed model was able to predict the behavior of HC-SCS columns under pure torsion. The Karagozian and Case Concrete Damage Model Release 3 (K&C model), with automatically generated parameters, produced good results for concrete modelling, including the modelling of high strength concrete. Parametric analysis was conducted by assuming the parameters and observing their influence on the T-θ curves. Six parameters influenced the column's torsion capacity. The outer steel tube's D/t_o ratio was the governing parameter that controlled the column's torsion capacity followed by concrete shell thickness and then the strength of the outer steel tube. The aspect ratio (H/D) of the column and inner steel tube's strength had low influence on the column's torsion capacity. All of the six columns had similar failure sequence. The only change in failure was change along the height of the column. The simplified analytical model developed based on parametric study was good in agreement with the experimental results.

Notation

The following symbols are used in this paper

D	Outer diameter of inner steel tube
D	Outer diameter of outer steel tube
f_{cu}	Characteristic 28-day concrete cube strength
f'_c	Unconfined compressive strength of concrete

f_{yi}	Yield strength of inner steel tube
f_{yo}	Yield strength of outer steel tube
J_{po}	Polar moment of inertia of outer steel tube
J_{pc}	Polar moment of inertia of concrete
J_{pi}	Polar moment of inertia of inner steel tube
t_o	Thickness of outer steel tube
t_i	Thickness of inner steel tube
T_{ue}	Experimental torsion strength (Huang et at., 2013)
$T_{FE, 0.01}$	Torsion strength predicted by FEA model
$T_{FE, u}$	Torsion capacity at failure of FE column
T_a	Torsion strength predicted by simplified analytical model
τ_{yo}	Shear stress of outer steel tube
τ_c	Shear stress of concrete
τ_{yi}	Shear stress of inner steel tube
θ	Twist

Acknowledgement

The research reported in the paper was supported by Missouri University of Science and Technology and National University Transportation Center (NUTC). The authors gratefully acknowledge their support. Any findings or conclusions are to the authors and do not reflect the sponsors.

References

Abdelkarim, O. and ElGawady, M. (2014a) "Behavior of Hybrid FRP-Concrete-Steel Double-Skin Tubes Subjected to Cyclic Axial Compression." *ASCE Structures Congress 2014*: pp. 1002-1013.

Abdelkarim, O. and ElGawady, M. (2014b). "Analytical and Finite-Element Modeling of FRP-Concrete-Steel Double-Skin Tubular Columns." *J. Bridge Eng.*, 10.1061/(ASCE)BE.1943-5592.0000700 , B4014005.

Abdelkarim, O., Geni, A., Anumolu, S., and ElGawady, M. (2015a). "Seismic Behavior of Hollow-Core FRP-Concrete-Steel Bridge columns." *ASCE Structures Congress*, pp. 585-596.

Abdelkarim, O. and ElGawady, M. (2015b). "Impact Analysis of Vehicle Collision with Reinforced Concrete Bridge Columns." *Transportation Research Board (TRB) conference*, Washington Dc, 15-4461.

ACI Committee 318 (2014). Building Code Requirements for Structural Concrete (ACI318-11) and Commentary (318R-11). *American Concrete Institute*, Farmington Hills, Mich.

Beck, J., and Kiyomiya, O. (2003). "Fundamental pure torsion properties of concrete filled circular steel tubes." *J. Materials, Conc. Struct. Pavements*, JSCE No. 739/V-60, pp. 85–96.

Belarbi, A., Prakash, S.S., and Silva, P. (2008). "Flexure-shear-torsion interaction of RC bridge columns." In: *Concrete bridge conference*. Paper no. 6.

Bi, K., Hao, H., and Ren, W.X. (2013). "Seismic Response of Concrete Filled Steel Tubular Arch Bridge to Spatially Varying Ground Motions Including Local Site Effect." Advances in Structural Engineering. 16(10).

Crawford, J. E., and Malvar, L. J. (2006). "User's and theoretical manual for K&C concrete model." Report TR-06-19.1, Karagozian and Case, Burbank, CA.

Dawood, H., ElGawady, M., and Hewes, J. (2012). "Behavior of Segmental Precast Post-Tensioned Bridge Piers under Lateral Loads." *ASCE Journal of Bridge Engineering*, Vol. 17, No. 5, pp. 735-746.

Dong, C.X., and Ho, J.C.M. (2012). "Uni-axial behaviour of normal-strength HC-SCS columns with external steel rings." Steel and Composite Structures, Vol. 13, No. 6, pp: 587-606.

Elchalakani, M., Zhao, X.L., and Grzebieta, R.H. (2002). "Tests of concrete-filled double skin CHS composite stub columns." *Steel and Composite Structures*. Vol. 13, No. 6, pp: 587-606.

Han, L.H., Huang, H., Tao, Z., and Zhao, X.L. (2006). "Concrete-filled double skin steel tubular (HC-SCS) beam – columns subjected to cyclic bending." *Engineering Structures*; 28(12):1698-1714.

Han, L.H., Yao, G.H., and Tao, Z. (2007). "Performance of concrete-filled thin-walled steel tubes subjected to pure torsion." *Thin-Walled Struct*; 45(1):24–36.

Hassanein, M.F., Kharoob, O.F., and Liang, Q.Q. (2013). "Circular concrete-filled double skin tubular short columns with external stainless steel tubes under axial compression." *Thin Walled structures*. Vol 73, pp: 252-263.

Huang, H., Han, L. H., and Zhao, X. (2013). "Investigation on concrete filled double skin steel tubes (CFDSTs) under pure torsion." *Journal of Constructional Steel Research*, Volume 90, 221-234.

Lee, G., Xu, J. S., Gong., A., and Zhang, K. C. (1991). "Experimental studies on concrete filled steel tubular short columns under compression and torsion." *Proc. 3rd Intl. Conf. on Steel-Concrete Composite Construction*, ACSCCS, Fukuoka, Japan, 143–148.

Lee, E., Yun, B., Shim, H., Chang, K., and Lee, G. (2009). "Torsional behavior of concrete-filled circular steel tube columns." *J.Struct. Eng.*, 135(10), 1250-1258.

Li, W., Han, L.H., and Chan, T. (2014). "Tensile behaviour of concrete-filled double-skin steel tubular members." *Journal of Constructional Steel Research*, Vol. 99, pp. 35-46.

Lin, M.L., and Tsai, K.C. (2001). "Behavior of double-skinned composite steel tubular columns subjected to combined axial and flexural Loads." *Proceedings of the First International Conference on Steel and Composite Structures*, Pusan, Korea, pp. 1145–1152.

Lu, H., Zhao, X., and Han, L.H. (2010). "Testing of self-consolidating concrete-filled double skin tubular stub columns exposed to fire." *Journal of Constructional Steel Research*, Vol. 66, Issues 8–9, pp. 1069-1080.

Malvar, L.J., Crawford, J.E., Wesevich, J.E., and Simons, D. (1997), "A plasticity concrete model for DYNA3D." Int. J. of Imp. Eng., vol. 19, No. 9-10, pp. 847-873.

Mullapudi, T.R.S., and Ayoub, A. (2012). "Analysis of Reinforced Concrete Columns Subjected to Combined Axial, Flexural, Shear and Torsional loads." *J. Structural Engineering*, 139(4).

Nie, J.G., Wang, Y.H., and Fan, J.S. (2012). "Experimental study on seismic behavior of concrete filled steel tube columns under pure torsion and compression–torsion cyclic load." *Journal of Constructional Steel Research*. 79:115–126.

Noble, C., Kokko, E., Darnell, I., Dunn, T., Hagler, L., and Leininger, L. (2005). "Concrete model descriptions and summary of benchmark studies for blast effects simulations." Lawrence Livermore National Laboratory (LLNL), Livermore, CA.

Mondal, T. G., and Prakash, S. S. (201a5). "Effect of tension stiffening on the behaviour of reinforced concrete circular columns under torsion." Engineering Structures, 92, 186-195.

Mondal, T. G., and Prakash, S. S. (2015b). "Nonlinear Finite-Element Analysis of RC Bridge Columns under Torsion with and without Axial Compression." Journal of Bridge Engineering, 04015037.

Prakash, S.S., and Belarbi, A. (2009). "Bending-shear-torsion interaction features of RC circular bridge columns—An experimental study. In: Thomas T.C. Hsu symposium on shear and torsion in reinforced concrete." SP-265, Paper No. SP-2. Farmington Hills, MI: American Concrete Institute.

Rabbat, B.G., and Russel, H.G. (1985). "Friction Coefficient of Steel on Concrete or Grout." *J.Struct. Eng*, Vol 111, No.3, Pg.505-515.

Roylance, D. (2001). "Yield and Plastic Flow." *Mechanics of Materials*, Department of Materials Science and Engineering, Massachusetts Institute of Technology, Cambridge, MA.

Ruili, H., Sneed, L.H., and Belarbi, A. (2014). "Torsional Repair of Severely Damaged Column Using Carbon Fiber-Reinforced Polymer." *ACI Structural Journal*, Vol. 111, No. 3.

Ryu, D., Wijeyewickrema, A., ElGawady, M., and Madurapperuma, M. (2014). "Effects of Tendon Spacing on In-Plane Behavior of Post-Tensioned Masonry Walls." *J. Struct. Eng*., 140(4), 04013096.

Tabor, D. (2000). "Hardness of Metals." Clarendon Press, Oxford.

Tao, Z., Han, L.H., Zhao, and X.L. (2004). "Behaviour of concrete-filled double skin (CHS inner and CHS outer) steel tubular stub columns and beam-columns." *Journal of Constructional Steel* , 60(8), 1129-1158.

Tao, Z., and Han, L. H. (2006). "Behaviour of concrete-filled double skin rectangular steel tubular beam–columns." *Journal of Constructional Steel Research*, *62*(7), pp. 631-646.

Wei, S., Mau, S.T., Vipulanandan, C., and Mantrala, S.K. (1995). "Performance of new sandwich tube under axial loading: Experiment." *ASCE Journal of Structural Engineering*, Vol. 121, No. 12, pp. 1806-1814.

Xu, J. S., Zhou, J., and Lee, G. (1991). "Experimental Studies on Concrete Filled Steel Tubular Medium and Long Columns under Compression and Torsion." *Proc. 3rd Intl. Conf. on Steel-Concrete Composite Construction*, ACSCCS, Fukuoka, Japan, 159–164.

Yagishita, F., Kitoh, H., Sugimoto, M., Tanihira, T., and Sonoda, K. (2000). "Double-skin composite tubular columns subjected cyclic horizontal force and constant axial force." *Proceedings of the Sixth ASCCS Conference*, Los Angeles, USA, March 22–24, pp. 497–503.

Youssf, O., ElGawady, M. A., Millsa, J. E., and Ma, X. (2014). "Finite element modelling and dilation of FRP-confined concrete." *Eng. Struct*., 79(Nov), 70-85.

Zhao, X.L., Han, B., and Grzebieta, R.H. (2002). "Plastic mechanism analysis of concrete-filled double-skin (SHS inner and SHS outer) stub columns." *Thin-Walled Structures*; 40(10): 815–33.

Zhao, X.L., Tong, L.W., and Wang, X.Y. (2010). "CFDST stub columns subjected to large deformation axial loading." *Engineering Structures*; 32(3):692-703.

Table 1. Summary of Columns Variables (reproduced after Huang et al. 2013)

Specimen label	Outer tube		Inner tube		f_{yo}, MPa (psi)	f_{yi}, MPa (psi)	f_{cu}, MPa (psi)
	D, mm (in.)	t_o, mm (in.)	d, mm (in.)	t_i, mm (in.)			
CO111	165 (6.5)	3.0 (0.12)	42 (1.65)	3.0 (0.12)	260.0 (37,700)	326.6 (47,357)	50 (7,250)
CO112		3.0 (0.12)	75 (2.95)	5.0 (0.20)	260.0 (37,700)	355.4 (51,533)	
CO211		4.0 (0.16)	42 (1.65)	3.0 (0.12)	286.4 (41,528)	326.6 (47,357)	
CO212		4.0 (0.16)	75 (2.95)	5.0 (0.20)	286.4 (41,528)	355.4 (51,533)	
CO311		4.6 (0.18)	42 (1.65)	3.0 (0.12)	365.6 (53,012)	326.6 (47,357)	
CO312		4.6 (0.18)	75 (2.95)	5.0 (0.20)	365.6 (53,012)	355.4 (51,533)	

Table 2. Summary of Experimental Results, FE, and Analytical Results

Column	T_{ue}, kN.m (k.ft.)	$T_{FE,0.01}$, kN.m (k.ft.)	T_a, kN.m (k.ft.)	% error in $T_{FE,0.01}$*	% error in T_a*	θ, experimental (°)	θ, FE (°)	% error in 'θ'
CO111	24.6 (18.1)	26.0 (19.2)	22.8 (16.8)	5.4	7.3	2.7	2.7	0
CO112	33.2 (24.5)	34.5 (25.4)	28.8 (21.2)	3.9	13.2	2.7	3.2	18
CO211	32.3 (23.8)	35.6 (26.3)	29.2 (22.9)	10.2	3.7	3.1	3.0	3
CO212	42.1 (31.1)	44.3 (32.7)	37.1 (27.4)	5.2	11.8	3.4	4.3	26
CO311	48.8 (36.0)	47.5 (35.0)	43.4 (32)	2.6	11.0	3.8	3.7	3
CO312	54.3 (40.0)	53.6 (39.5)	49.3 (36.4)	1.3	9.2	3.5	3.5	0

* The percentage of the absolute value of the difference between the experimental and the FE/Analytical torsion strengths divided by the experimental torsion strength

Table 3. Outer Steel Tube Shear Stress and the Torsion Capacity at Failure

Column	Failure shear stress at outer steel tube, MPa (psi)	Torsion capacity, kN.m (kip.ft)
CO111	191 (27,702)	33.3 (24.5)
CO112	190 (27,557)	41.7 (30.7)
CO211	202 (29,297)	44.3 (32.6)
CO212	205 (29,732)	51.9 (38.2)
CO311	249 (36,114)	56.5 (41.6)
CO312	248 (35,969)	64.4 (47.5)

Table 4. Summary of Parametric and Analytical Results

Parameter	Parametric value	FE, T_{FE}		Analytical, T_a	
		KN.m	k-ft	KN.m	k-ft
f_{yo}	310 MPa (45 ksi)	38.7	28.5	32.9	24.3
	380 MPa (55 ksi)	44.4	32.5	38.0	28.0
	448 MPa (65ksi)	47.2	34.8	42.2	31.1
	586 MPa (85 ksi)	53.7	39.6	53.0	39.1
f_{yi}	310 MPa (45 ksi)	42.4	31.2	36.4	26.8
	380 MPa (55 ksi)	44.4	32.7	38.0	28.0
	448 MPa (65ksi)	44.6	32.9	39.2	28.9
	586 MPa (85 ksi)	44.7	32.9	42.1	31.1
f'_c	10 MPa (1.5 ksi)	39.6	29.2	37.4	27.6
	40 MPa (5.8 ksi)	44.4	32.7	38.0	28.0
	70 MPa (10.2 ksi)	44.5	32.8	38.5	28.4
	100 MPa (14.5 ksi)	44.7	32.9	39.0	28.7
t_c	15 mm (0.6 in.)	61.3	45.2	58.9	43.4
	30 mm (1.2 in.)	49.7	36.6	48.3	35.6
	45 mm (1.8 in.)	44.4	32.7	38.0	28.0
	100 mm (2.9 in.)	35.3	26.0	35.0	25.8
D/t_o	15	107.0	79.0	111.5	82.3
	60	34.6	25.5	33.0	24.3
	120	26.4	19.5	22.9	16.9
	200	18.3	13.5	17.9	13.2
	250	16.9	12.5	16.3	12.1
d/t_i	15	44.4	32.7	38.0	28.0
	60	36.3	26.7	32.2	23.7
	120	35.0	25.8	31.1	22.9
	200	34.3	25.3	30.6	22.6
	250	33.9	25.0	30.5	22.5

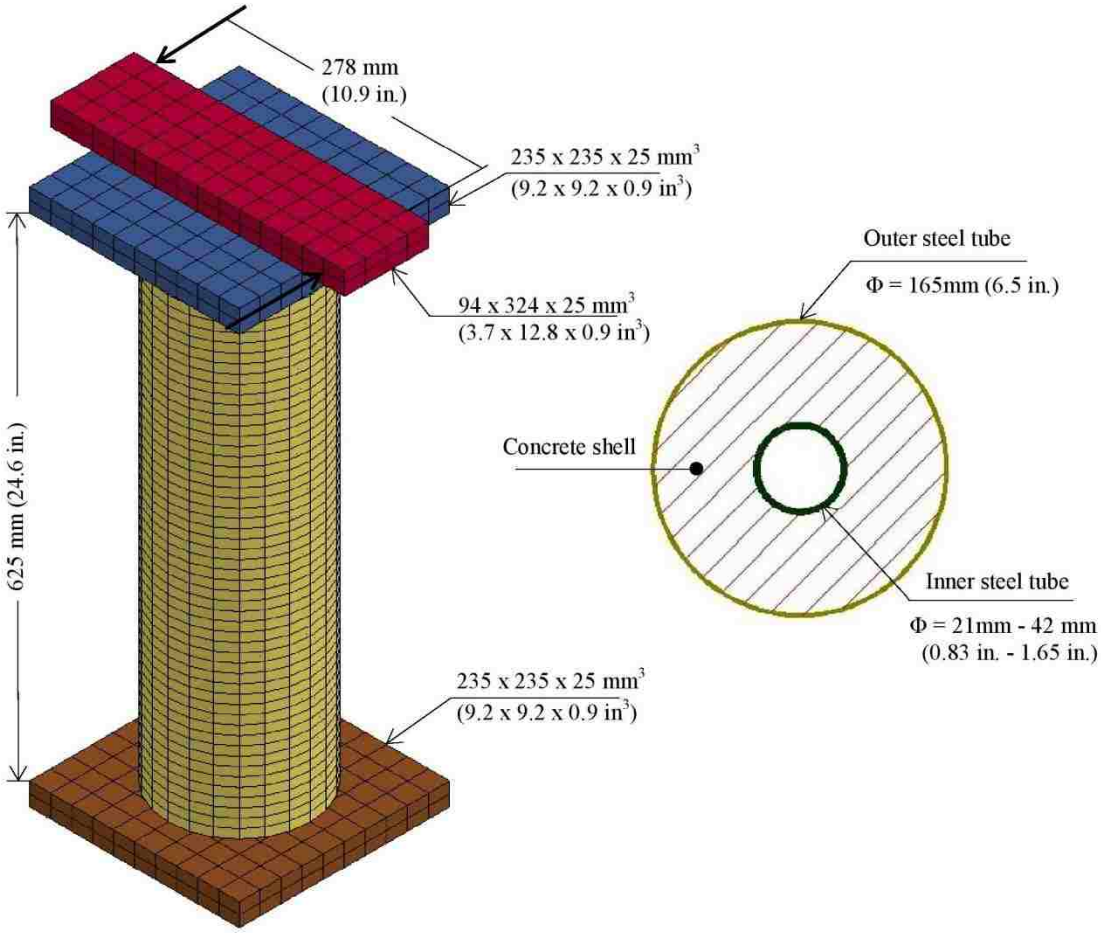

Fig. 1. (a) FE Model of HC-SCS Column, (b) Cross-section View of HC-SCS Column

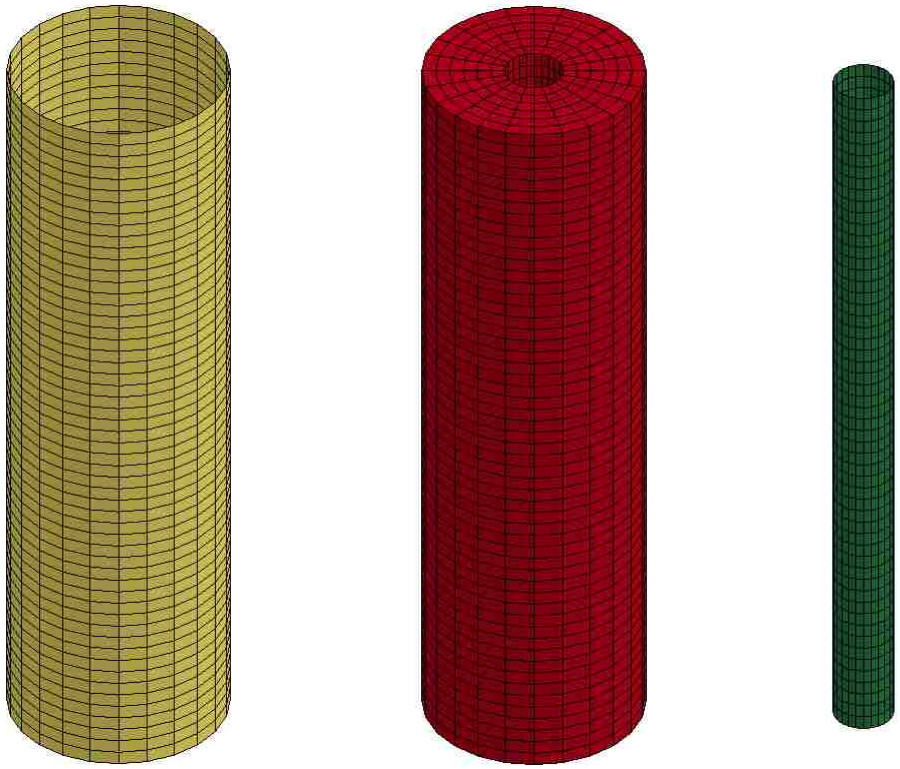

(a) (b) (c)

Fig. 2. FE Model Components: (a) Outer steel tube, (b) Concrete Shell, (c) Inner Steel Tube

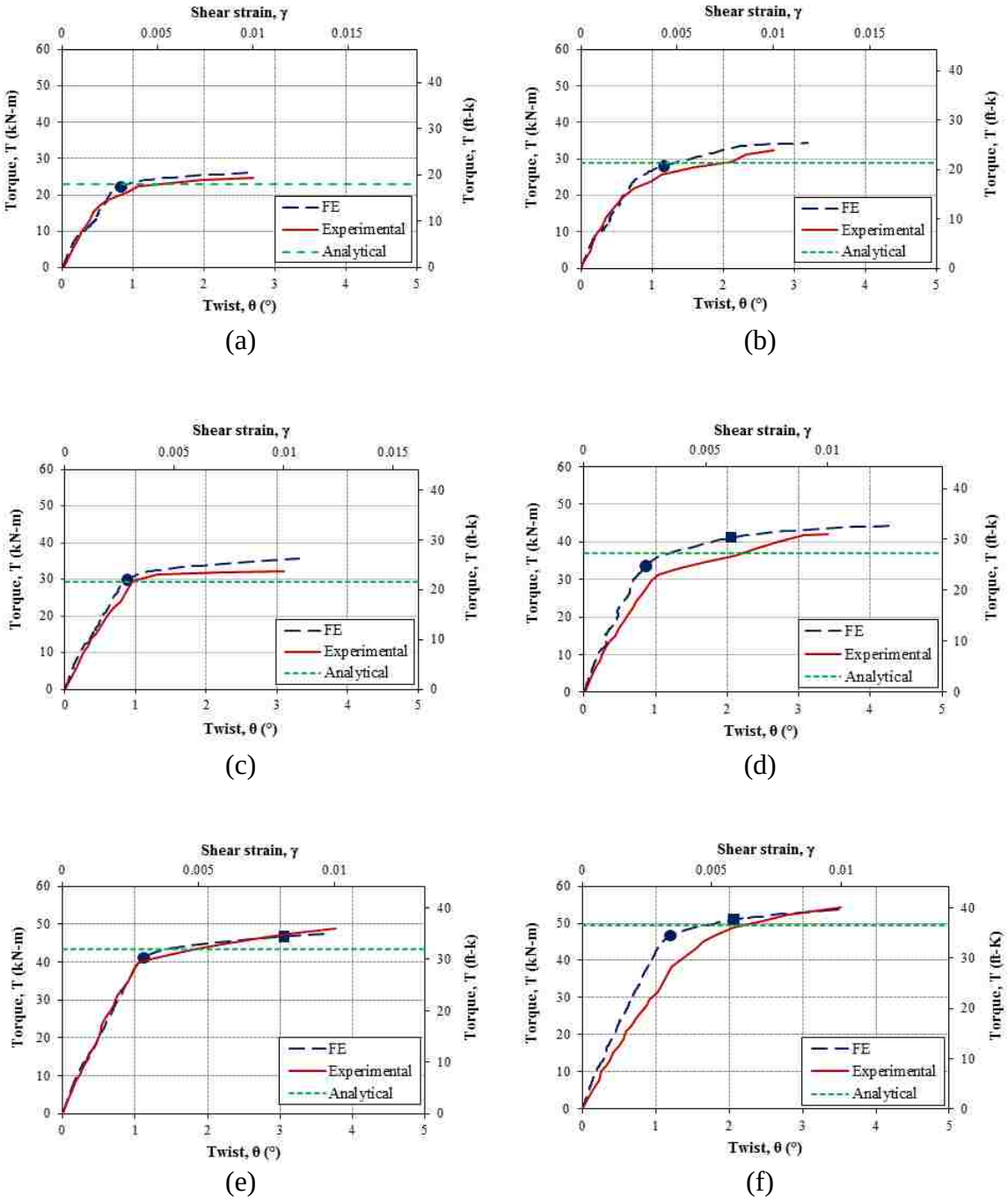

Fig. 3. Experimental (Huang et al. 2013) vs. FE Backbone Curves for Specimens: (a) CO111, (b) CO112, (c) CO211, (d) CO212, (e) CO311, and (f) CO312

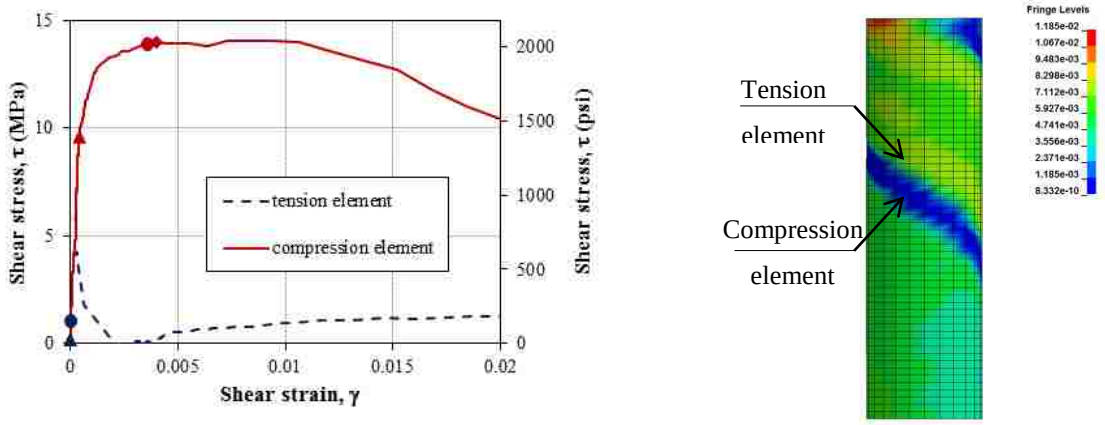

(a) (b)

▲ Yielding in outer steel tube ● yielding in inner steel tube

◆ 0.01 shear strain in outer steel tube

Fig. 4. (a) Typical Shear Stress- Shear Strain Relation of Two Concrete Elements, (b) Confined Concrete Shear Stress at the Initial Shear Crack for Column CO211 in GPa

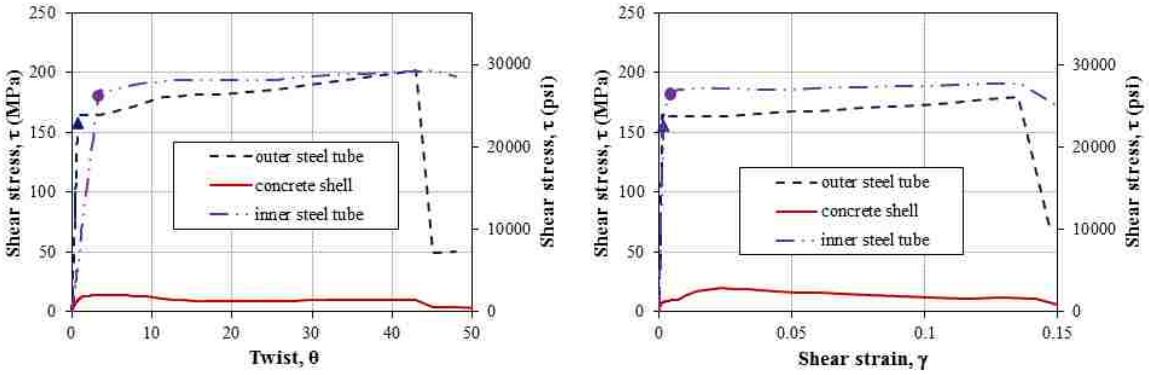

(a) (b)

▲ Yielding in outer steel tube ● Yielding in inner steel tube

Fig. 5. Behavior of Steel Tubes and Concrete Shell at 550 mm (21.65 in.) Height of Column CO211 (a) Shear Stress versus Twist; (b) Shear Stress versus Shear Strain

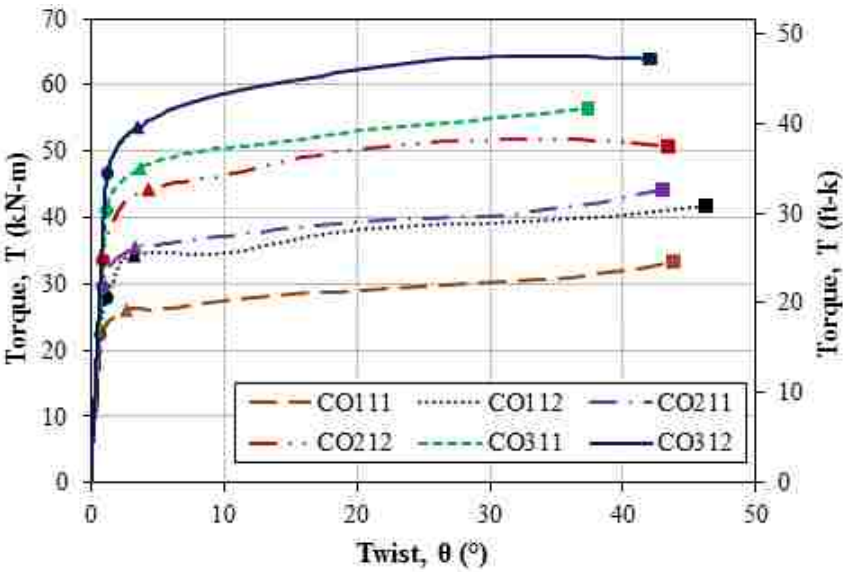

● Yielding of outer steel tube ▲ Torque capacity of FE column
■ Ultimate torsion moment of FE column

Fig. 6. FE Backbone Cure for Torque vs. Torsional Angle till the Failure

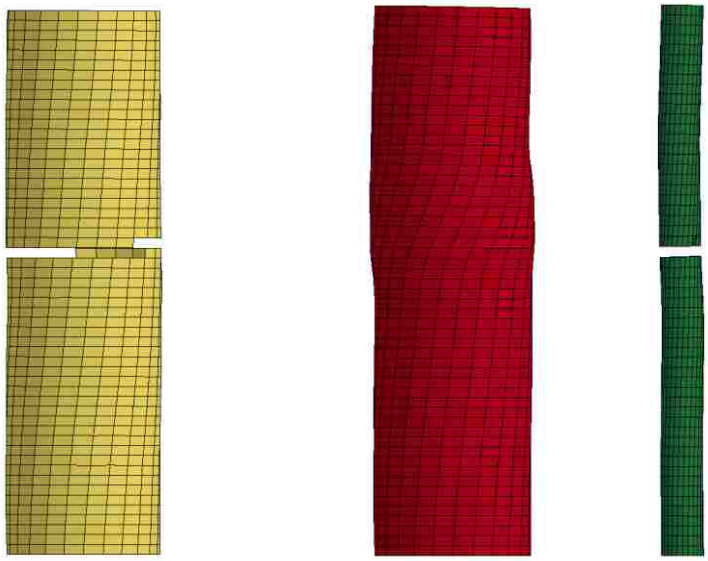

(a) (b) (c)

Fig. 7. Typical Mode of Failure of FE Columns (a) Outer Steel Tube, (b) Concrete Shell, and (c) Inner Steel Tube

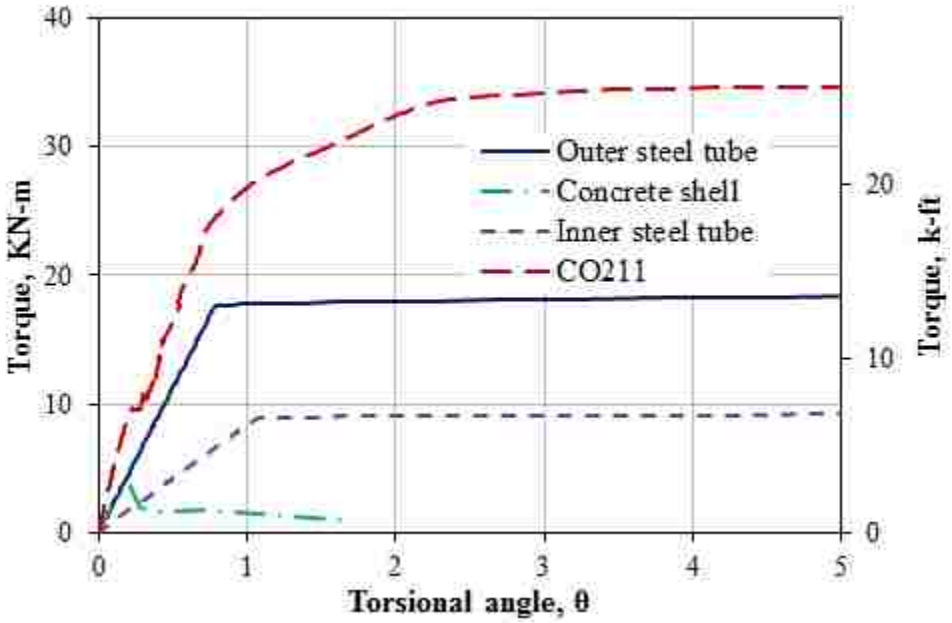

Fig. 8. Typical Contribution of Steel Tubes and Concrete Shell towards Torque Capacity for the Column CO112

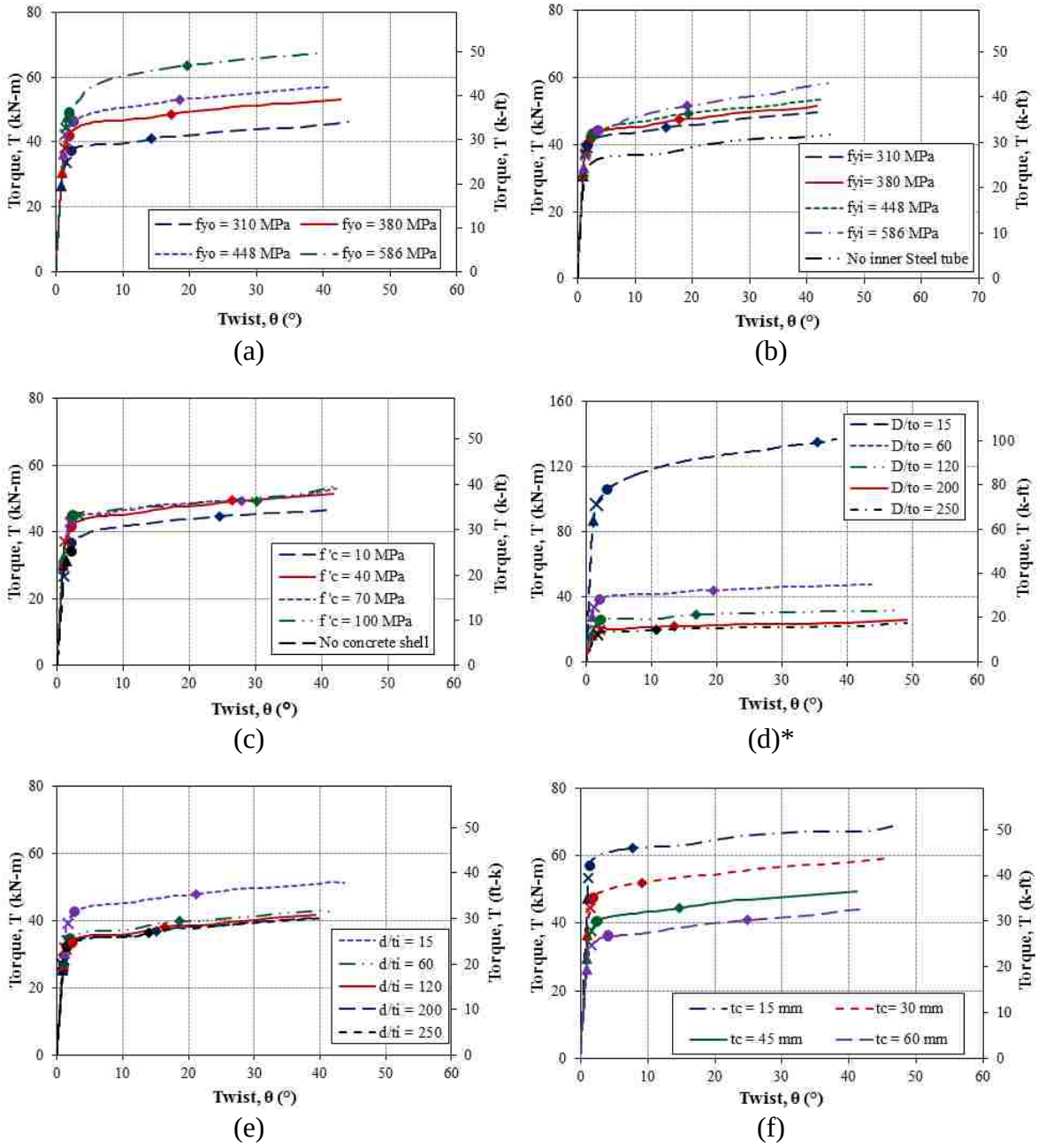

▲ Yielding in outer steel tube ● Yielding in inner steel tube

X Compressive strength of concrete ◆ Confined compressive strength of

* The scale of the curve is different

Fig. 9. Effect of Parameters on the Torsional Behavior of HC-SCS Column

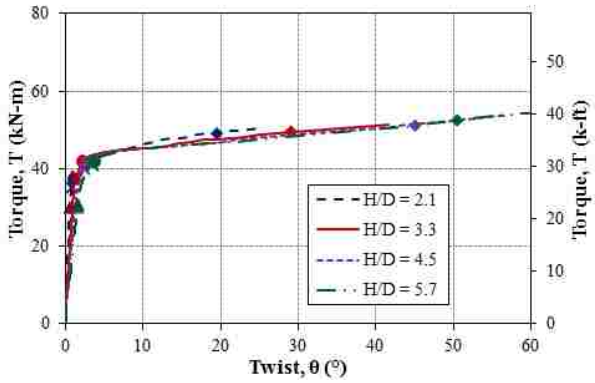

(g)

▲ Yielding in outer steel tube
● Yielding in inner steel tube
X Compressive strength of concrete
◆ Confined compressive strength of

* The scale of the curve is different

Fig. 9. Effect of Parameters on the Torsional Behavior of HC-SCS Column (CONTINUED)

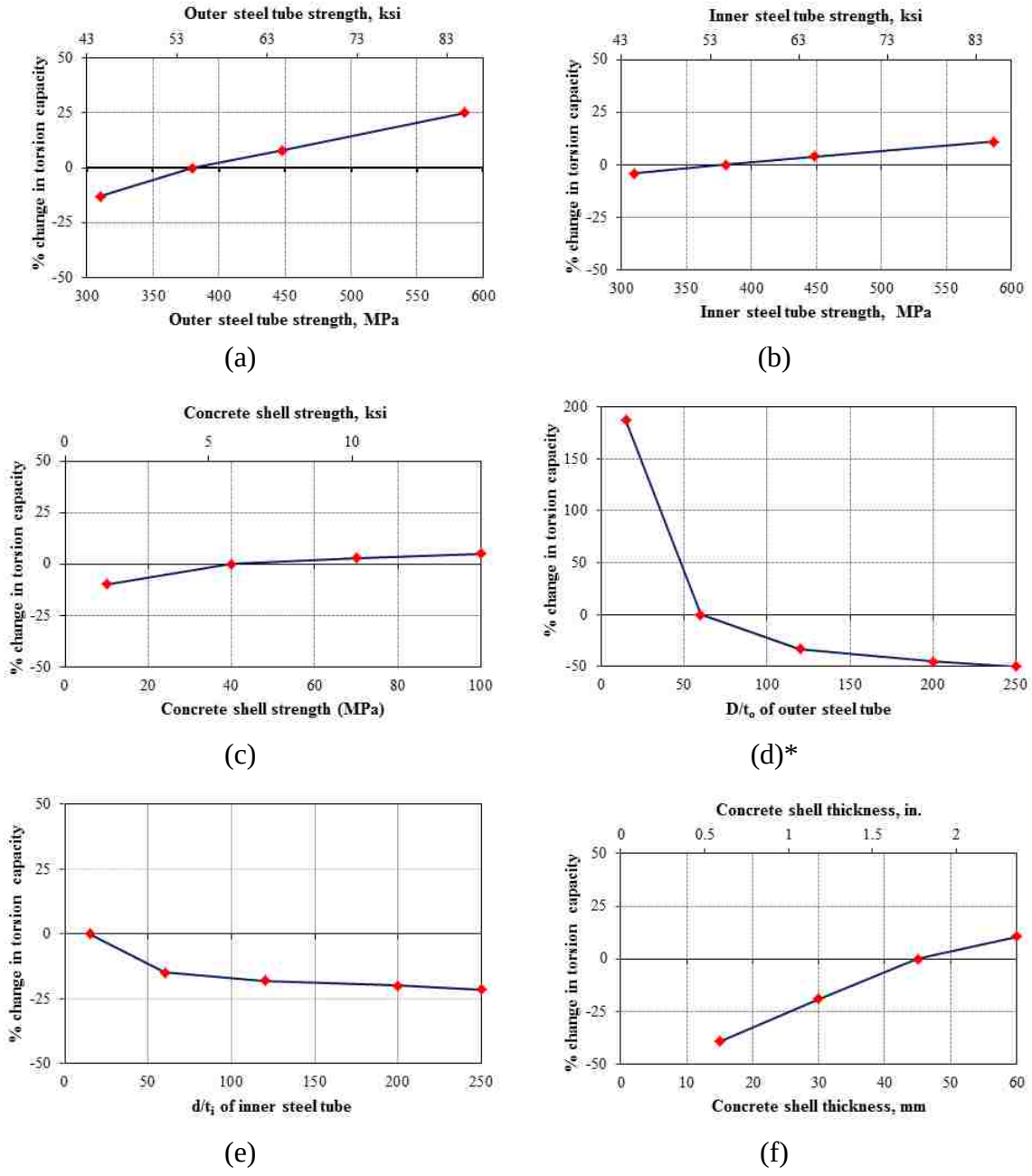

* The scale of the curve is different

Fig. 10. Percentage Change in Ultimate Torsion Moment of HC-SCS Column due to Change: (a) f_{yo}, (b) f_{yi}, (c) f'_c, (d) D/t_o, (e) d/t_i, (f) t_c, and (g) H/D

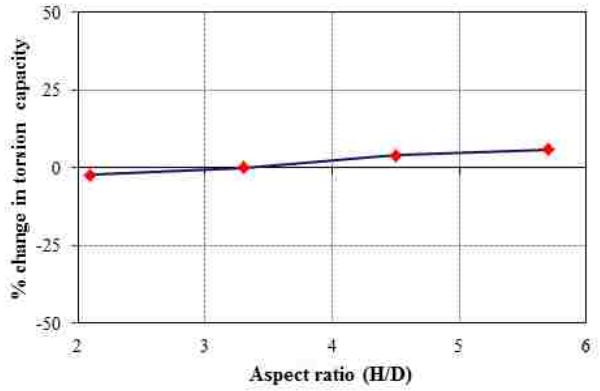

(g)

Fig. 10. Percentage Change in Ultimate Torsion Moment of HC-SCS Column due to Change: (a) f_{yo}, (b) f_{yi}, (c) f'_c, (d) D/t_o, (e) d/t_i, (f) t_c, and (g) H/D (CONTINUED)

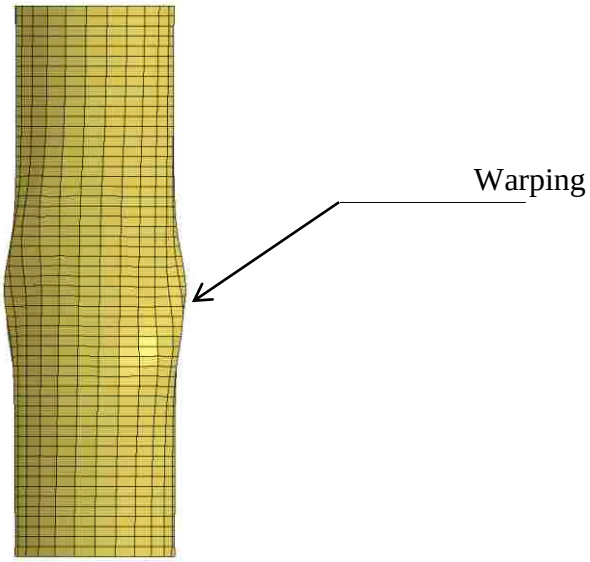

Fig. 11. Warping in Outer Steel Tube

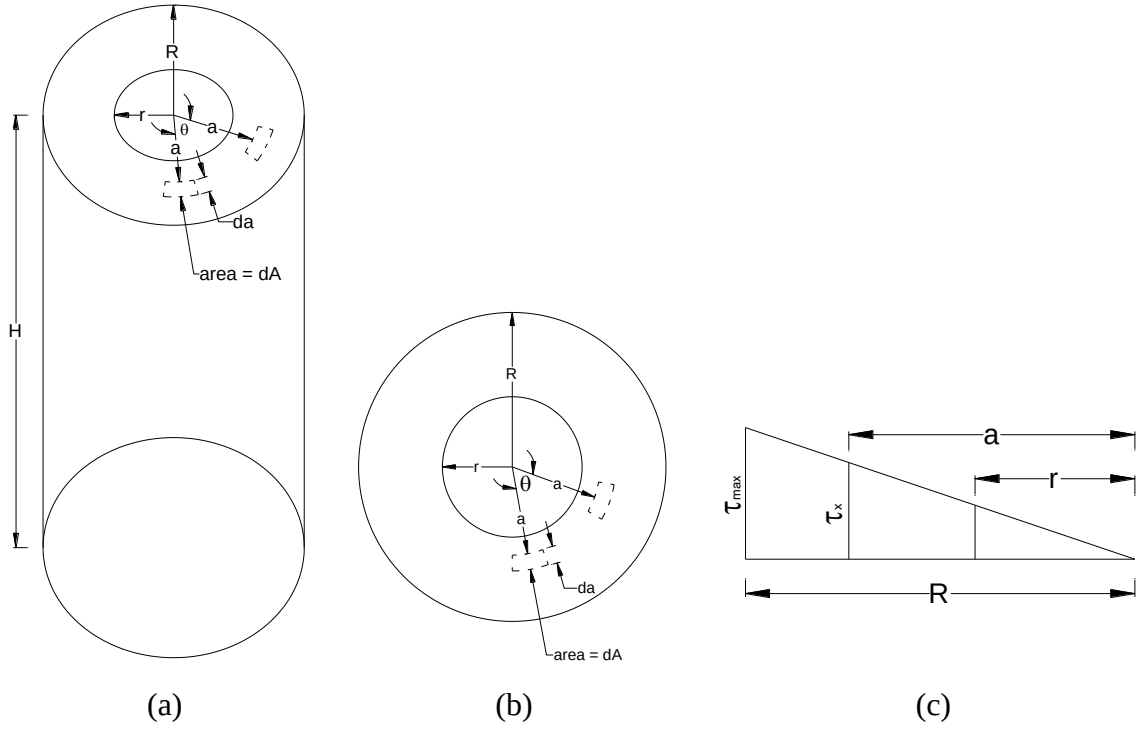

(a) (b) (c)

Fig. 12. Torsional Terms on Concrete Shell (a) Isometric View, (b) Cross-Section View, and (c) Shear Stress Variation along the Radius

II. Torsional Behavior of Hollow-Core FRP-Concrete-Steel Columns

Sujith Anumolu[1], S.M. ASCE; Omar I. Abdelkarim[2] S.M. ASCE; Mohanad Abdulazeez[3] S.M. ASCE; Ahmed Gheni[4] S.M. ASCE; Mohamed ElGawady[5$], PhD, M. ASCE

Abstract

This paper presents the behavior of hollow-core fiber reinforced polymer-concrete-steel (HC-FCS) column under pure torsion with constant axial load. The HC-FCS consists of outer FRP tube and inner steel tube with concrete shell sandwiched between the two tubes. The FRP tube was stopped at the surface of the footing and provides confinement to the concrete shell from outer direction. The steel tube was embedded into the footing to a length of 1.8 times to the diameter of the steel tube. The longitudinal and transversal reinforcements of the column were provided by the steel tube only. A large-scale HC-FCS column was investigated for this study. The study revealed that the torsional behavior of HC-FCS column mainly depends on the stiffness of the steel tube and the surface interactions (ie., cohesion, friction) occurred between the steel tube and the concrete. The contribution of FRP tube towards torsional capacity was small and negligible. A brief comparison was made between the reinforced concrete column and HC-FCS column in terms of stiffness and ductility. The HC-FCS column performed

1 Graduate Research Assistant, Dept. of Civil, Architectural, and Environmental Engineering, Missouri University of Science and Technology, Rolla, MO. 65401; sat6f@mst.edu
2 Ph.D. Candidate, Dept. of Civil, Architectural, and Environmental Engineering, Missouri University of Science and Technology, Rolla, MO. 65401; oiafgc@mail.mst.edu
3 Graduate Research Assistant, Dept. of Civil, Architectural, and Environmental Engineering, Missouri University of Science and Technology, Rolla, MO. 65401; mma548@mail.mst.edu
4 Ph.D. Candidate, Dept. of Civil, Architectural, and Environmental Engineering, Missouri University of Science and Technology, Rolla, MO. 65401; aagmr6@mst.edu
5Benavides Associate Professor, Dept. of Civil, Architectural, and Environmental Engineering, Missouri University of Science and Technology, Rolla, MO. 65401; elgawadym@mst.edu
§Corresponding author

better than the reinforced concrete column in terms of ductility but similar in terms of stiffness.

Keywords: Hollow-core; Torsion loading; Composite column; FRP

Introduction

Usually bridge columns are subjected to flexural and shear loading during earthquakes. However, the columns in bridges with curved or skewed superstructures are subjected to torsional loading as well. Developing of new type of bridge system had been focused by several researchers to reduce the seismic effects along with achieving construction acceleration. Accelerated bridge construction technology has been developed in cost effective manner to decrease the on-site construction time and enhance work-zone safety (Dawood et al. 2012; Abdelkarim and ElGawady 2015a).

Concrete-filled steel tubes are developed as an initiative to accelerating bridge construction in 1960s. This system significantly decreases the reinforcement detailing and workmanship for the construction. The presence of steel tube surrounding the concrete acts as permanent formwork, longitudinal and transversal reinforcement, and improves confinement to concrete core. The concrete core acts as bracing to the steel tube and provide lateral stability that delays or prevent local buckling in steel tube. The combination of two materials, steel tube and concrete enhances strength and ductility of the column. The material costs of concrete-filled steel tubes was slightly higher compared to reinforced concrete columns and lower compared to steel columns. The practical application of concrete-filled steel tube were used as bridge columns in Europe, China

and Japan and extended to the US. as piles. However, due to lack of design provision, the use of concrete filled steel tubes was limited (Moon et al. 2013).

The fiber reinforced polymer (FRP) with high strength was used in place of steel and a new system was developed known as concrete-filled fiber tubes were developed by Mirmiran and Shahawy 1996 had gained importance. The orientation of fiber in multi-direction exploits the use of FRP as longitudinal and transverse reinforcement to the column, improves the energy dissipation and decreases the reinforcement detailing. The corrosion resistance and confinement to the concrete core were improved by using fiber in place of steel. Several researchers had investigated the concrete-filled FRP tube different loadings (ElGawady et al. 2010; Dawood and ElGawady 2013; Fam et al. 2003; Ozbakkaloglu 2012; Mirmiran et al. 2001; Lam and Teng 2004; Zhu et al. 2005; Dai et al. 2011). The study reveals concrete-filled FRP exhibited high strength and ductility compared to reinforced concrete columns under seismic loadings.

The lateral stiffness of a bridge is the controlling factor in seismic design since the typical bridge column would sustain 5% to 10% of its axial load capacity. Montague et al. (1978) has advanced the concrete filled steel tube by making hollow in the center of the column known as hollow-core steel-concrete-steel columns. The hollow-core steel-concrete-steel columns consist of concrete shell sandwiched between two steel tubes. The self-weight and section modulus of the column were decreased and the stiffness of the column was increased which were important parameters in achieving cost-effective pre-cast construction. Furthermore, the inertial forces will be reduced with column weight in long columns. Teng et al. (2004) developed a new system of hollow-core FRP-concrete-steel columns (HC-FCS) by exploiting the advantage of using three materials FRP,

concrete, and steel. Fiber tube was used as outer tube in the HC-FCS column. The HC-FCS column stiffness and ductility were enhanced by combination of FRP and steel, respectively. The orientation of fiber close to the hoop direction prevents the local bucking of outer tube. The HC-FCS column under monotonic axial load showed the improvement in confinement to concrete shell and delay of local buckling in steel tube. The HC-FCS column's fire resistance was improved compared to concrete-filled tubes. The FRP tube and concrete core prevents the corrosion of inside steel tube. Several researchers had investigated the HC-FCS column under different loadings (Teng et al. 2007; Abdelkarim and ElGawady 2014a,b; Yu et al. 2006; Wong et al. 2008; Ozbakkaloglu and Akin 2001; Zhang et al. 2015). The HC-FCS columns exhibited high levels of energy dissipation before the rupture of FRP tube. Recently, large-scale HC-FCS columns were tested by Abdelkarim et al. (2015b) under combined axial and flexural loads. They reported that the HC-FCS columns reached to a high lateral drift compared to reinforced concrete column.

The torsional loads are significant during earthquakes for skewed and curved bridges in addition to the asymmetric structures with different eccentric load action. However, there was no practical existence of pure torsion as it combines with axial and/or flexural loads. The pure torsional studies were necessary to assess the column behavior under combined loadings. Ostuska et al. (2004) and Prakash et al. (2009) had investigated the reinforced concrete column under pure torsion and reported that the locking and unlocking of spiral reinforcement in reinforced concrete had significantly affected column's torsional behavior under cyclic loading. Moreover, the spalling of concrete was higher during unlocking of spiral compared to locking of spiral.

For concrete-filled steel tubes, during torsional loading the concrete core resists compression force while the steel tube resists tension force forming a truss action. Beck and Kiyomiya (2003) had investigated the pure torsional behavior of concrete-filled steel tubes and reported that the buckling of steel tube was avoided due to the concrete core and the column maintained high stiffness and ductility compared to steel and reinforced concrete columns. Han et al. (2007a) investigated the torsional behavior of concrete-filled steel tube and reported that the concrete core has significant effect on the column's torsional resistance and developed a theoretical model to calculate the column's torque. Other researchers (Gong 1989; Lee et al. 1991; Xu et al. 1991; Han et al. 2007(b) and Nie et al. 2012) had investigated torsion behavior of concrete-filled steel tubes under static cyclic combined axial and/or bending loads including torsion.

Recently, Huang et al. (2013) investigated the hollow-core steel-concrete-steel columns under pure torsion and reported good energy dissipation of column along with strength and ductility. Based on the influential parameters affecting the torsional behavior of hollow-core steel-concrete-steel columns, Huang et al. (2013) proposed design formula for calculating the torsional capacity. A conclusion from above reviewed literature, concrete-filled steel tubes and hollow-core steel-concrete-steel columns exhibited good strength and ductility compared to reinforced concrete and steel columns.

The current study introduces the behavior of HC-FCS column under combined cyclic torsional loading and constant axial load. A large scale HC-FCS column was built and investigated for this study. The study on effects of friction between the steel tube and concrete was studied. The general torsional behavior of the reinforced concrete column and HC-FCS column were compared.

Experimental Program

Test Specimen

A large-scale HC-FCS column was constructed and tested under combined cyclic torsional loading and constant axial load. The column dimensions and cross-sectional details were shown in Fig. 1. The column's actual height between the surfaces of the footing and the loading head was 80 in. (2032 mm). The column's effective height from the surface of the footing to the center line of applied torsional load was 96 in. (2438 mm) representing an aspect ratio of 4. The outer FRP tube (D) and inner steel tube (d) diameters of the column were 24 in. (610 mm) and 14 in. (355 mm), respectively. The thickness (t_o) of the FRP tube was 0.446 in. (11 mm). The thickness (t_i) of the steel tube was 0.25 in (6.35 mm) representing diameter-to-thickness (d/t_i) ratio of 56. The percentage area of steel reinforcement in both longitudinal and transverse for the column in form of steel tube was 3.5%. The embedded length of the steel tube into the footing was 1.8 times the diameter of the steel tube. The FRP tube was stopped between the surfaces of the footing and the loading head. Table 1 summarizes the variables of the column.

The dimension of the footing was 60 in. (1524 mm) in length, 48 in. (1219 mm) in width, and 34 in. (863 mm) in depth. The reinforcing detail of the column was shown in Fig. 1. A total of 6 #7 steel rebars as top reinforcement, 7 #7 steel rebars as bottom reinforcement, and 20 #4 steel rebars as shear reinforcement was provided to the footing. A steel stand with height 9 in. (228 mm) was constructed to place the steel tube inside the footing and to provide embedded length (25 in. (635 mm)) for the steel tube. The dimension of the loading head was 30 in. (762 mm) in length, 30 in. (762 mm) in width,

and 34 in. (863 mm) in depth. A clear cover of 1 in. (25.4mm) spacing was maintained on all sides of the footing and the loading head.

Material Tests and Properties

The FRP tube was manufactured by carbon fiber using epoxy as resin. The fiber orientation was $\pm 55°$ to the hoop direction of the tube. Tensile tests were carried out on the FRP coupons to ensure the manufacturer properties. The coupons were cut along the longitudinal length of the FRP tube. Two strain gauges were attached to at the middle height of the coupon to measure strain in the readings (Fig. 2). The coupon tests on FRP were carried out based on the guidelines provided from ASTM D3039. The loading rate for the test was maintained at 0.05 in./min (1.27 mm/min). The coupons failed around the middle region along the fiber orientation (55°). The coupon test results were different from the manufacturer's data due to de-bonding between the fiber layers and insufficient width of the coupons that terminate the fiber in radial direction. Table 2 summarizes the mechanical properties of FRP tube provided from manufacturer's data sheet.

The concrete mixed proportions were designed based on the required strengths. The coarse aggregate used only for the column's concrete shell was pea gravel with maximum aggregate size of 3/8 in. (9 mm). The water-cement (w/c) ratio was maintained at 0.5 for all the concrete members. The workability of the concrete shell was increased by the usage of High Range Water Reducers (HRWR). The mixed proportions of concrete were summarized in Table 3. The concrete cylinders of the concrete shell and the footing were tested at 28 days and date of test to measure the unconfined compressive strength. The summary of test results was in Table 4.

Tension tests were conducted on the steel coupons obtained from the longitudinal direction of the steel tube. The tests were carried on universal testing machine with 0.05 in./min (1.27 mm/min) constant loading rate (Fig. 2). The properties of steel tube provided from the coupon test results was shown in Table 5. The steel coupon tests were carried based on the ASTM A370 guidelines. The summary of test results was shown in Table 5. The steel coupons failed by necking after yielding.

Experimental Setup and Instrumentation

Two servo-controlled hydraulic horizontal actuators from north direction were used to apply cyclic torsional load (Fig. 3). The axial load was applied on the loading head through automatic hydraulic jacks to keep the axial load constant during applying the torsional loading (Fig 3). The load cells were placed between the loading head and hydraulic jacks to monitor the applied axial load. The axial load was transferred from hydraulic jack to the column through six un-bonded high strength pre-stressed strands. Fig. 3 illustrates the test setup.

A total of 48 strain gauges were attached on the FRP tube at six levels with spacing of 5 in. (127 mm) started from the surface level of footing to 25 in. (635 mm) along the height of the column. At each level, total of 8 strain gauges with 4 on hoop direction and 4 on vertical direction were attached on east, west, north and south directions, respectively. A total of 56 strain gauges were attached on the steel tube at seven levels with spacing of 5 in. (127 mm) started from 15 in. (381 mm) bottom of the steel tube to 45 in. (635 mm) from bottom of the steel tube along the height of the column. At each level, total of 8 strain gauges with 4 on hoop direction and 4 on vertical direction were attached on east, west, north and south directions, respectively. Two Strain rosettes were

attached on the steel tube at the surface level of the footing and 5 in. (127 mm) above it on north direction. Each strain rosette measures shear strain along with longitudinal strain and hoop strain. The buckling behavior of steel tube and slip of steel tube over concrete were monitored using cameras fixed inside the steel tube. Total of three cameras were fixed inside the steel tube along with light bulbs to provide illumination. The cameras were positioned at the top and bottom of the steel tube and at the surface level of the footing. The twist of the column which was measured at the load point on the loading head and twist of the FRP tube were measured using string potentiometers. Total of 6 string potentiometers were attached at different location over the column height. LVDTs were used to measure rocking, sliding of footing and slip of FRP tube over the loading head. The detailed instrumentation of the column was shown in Fig. 4

Rotation Measurement

Rotation of FRP Tube by String Potentiometer

A string of length 'L' from the string potentiometer was attached to the column (Fig. 5a). The application of torsional load rotates column to a twist angle of 'θ'. The length of the string from string potentiometer changes to 'L′'. The radius of the column was assumed to be 'R'.

$$\text{According to cosine rule, } Cos\ \theta = \frac{(L+R)^2+R^2-L'^2}{2*L*R} \quad (1)$$

$$\text{From Eq. 1, } \theta = Cos^{-1}\left(\frac{(L+R)^2+R^2-L'^2}{2*L*R}\right) \quad (2)$$

Twist Angle of the Column by LVDT

From the Fig. 5(b), the distance between the two LVDTs on the loading head was 'a'. The column was rotated to a twist angle of 'θ' and 'Δ_1' and 'Δ_2' are the respective displacements of LVDTs.

$$\text{The twist angle of the column, } \theta = Tan^{-1}\left(\frac{\Delta 1+\Delta 2}{a}\right) \quad (3)$$

Loading Protocol

The axial load of 55 kips (245 kN) was applied on each hydraulic jack with a total axial force of 110 kips (490 kN) that represents 5% axial capacity of the reinforced concrete column with same outer diameter and 1% longitudinal reinforcement. The axial load was maintained constant throughout the test and was monitored by load cells.

The torsional load was applied through two servo-controlled hydraulic horizontal actuators from north direction. Displacement control was adopted to apply the torsional load on the column. The displacements of the two actuators were maintained at equal and opposite direction. The loading regime of the actuators was based on the FEMA 2007 recommendations in which the displacement amplitude of the each actuator was 1.4 times the previous displacement. Each of the displacement amplitude comprises of two cycles and frequency of each displacement cycle was set to 50 Hz. The displacement rate of the each actuator was varied between 0.01 in./sec (0.25 mm/sec) to 0.04 in./sec (1.00 mm/sec). The loading regime used for cyclic torsional loading was shown in Fig. 6.

Results and Discussion

General Behavior

The torque – twist hysteretic curve of the HC-FCS column was shown in Fig. 7. The torque of the column was calculated by the summation of forces obtained from each actuator through load cells multiplied by half of the distance between the actuators which was 18 in. (457 mm). The actual twist of the column was obtained by subtracting the sliding effects of the footing during the test from the twist of the column. The twist of the FRP tube was calculated along the height of the column. The column's torque of the hysteresis curve showed abnormal deviation after 7° column's twist due to additional force provided from the actuator (Fig. 7). The additional force was due to the rotational constrained of the actuator arm. The column reached torque of 128 kip-ft (173.5 kN.m) in positive cycle and 135 kip-ft (185 kN-m) in negative cycle at 7° twist. A curve with dotted lines was graphed in Fig. 7 to show an ideal behavior of column after removing the additional force provided from the actuator. Through the ideal curve shown in Fig. 7, the ultimate torque carried by the column was extended to 146 kip-ft (198 kN-m) at 13.3° twist in the column.

The column gained early stiffness and reached 70% of the column's ultimate torque at 0.5° twist in the column. The cohesion loss occurred between the loading head and concrete shell at 0.5° twist resulted slight degradation in the torque-twist curve, however the drop was very low (Fig. 8). After the loss of cohesion, the torque carried by the column was mainly depended on the stiffness of the steel tube and frictional force exerted between the concrete elements (footing, concrete shell, and loading head) and steel tube. The torque of the column continued to increase at smaller increments with the column's

twist after the loss of cohesion due to the stiffness of the steel tube and existed frictional force between steel tube and concrete shell. Since there was no firm fixation of FRP tube in axial direction, the contribution of FRP tube towards torsional resistance was negligible. The presence of confinement and rigidity of FRP tube itself allows the rotation of FRP tube along with the concrete shell. The rigid rotation of FRP tube with concrete shell was observed during the experimentation.

Since the column lost cohesion at 0.5° twist, the drop in the curve at 3.5° column's twist in negative cycle was due to sudden sliding of steel tube over the footing (Fig. 8). The sudden sliding was noticed by the cameras fixed inside the steel tube at negative 3.5° twist. The sudden sliding started at higher rotational cycles of the actuator. However, the torque continued to increase due to gain in frictional force between the steel tube and the concrete. The gain in friction force was due to small deformations in the steel explained later in the manuscript. At higher rotational levels, the column's torque mainly depends on the friction exerted between the concrete and the steel tube.

The FRP tube was removed to observe the cracks on the concrete shell. The cracks were propagated throughout the height of the column at an angle of 45° (Fig. 9). The maximum crack width on the concrete shell was 0.8 in. (2 mm) which occurred at the top region of the column. Significant amount of cracks were observed at the bottom of the column compared to top of the column. The frictional force exerted between the footing and concrete shell was higher compared to concrete shell and loading head. The additional axial force on the footing in the form of column's self-weight endeavors high friction between the concrete shell and the footing. The high friction between the footing and the concrete shell constrain rotation of concrete shell over footing whereas, low

friction between concrete shell and loading head allows rotation of loading head over concrete shell. The contact surfaces of the loading head and the concrete shell became smooth at the end of the test. The loading action in both directions grinded the concrete surfaces and made smooth shown in Fig. 10. The contact surfaces of the footing and the concrete column were still rough confirming the high friction exerted between the contact. The steel tube was still in intact with the concrete surfaces. No visual deformations were observed on the steel tube.

FRP and Steel Tube Sliding over the Concrete Shell

The elevation view of the tested HC-FCS column under torsion loading at 9° twist was shown in Fig. 11a. The twist between the FRP tube with concrete shell and loading head was relative (Fig. 11b, Fig. 12). The relative sliding between the steel tube - concrete shell, and concrete shell - loading head caused relative twist between the FRP tube with concrete shell and loading head. The relative twist between the FRP tube with concrete shell and loading head had been noticed from the small twists of the column.

Since, lack of rigid fixation of FRP tube at both the ends, the rotation along FRP tube height remains constant (Fig. 12). In Fig. 12, the twist of FRP tube was almost half of the twist of the column at higher degrees of rotation. The relative twist was calculated between the column which was measured at the load point and the FRP tube. The relative twist was ratio of difference in twist of the column and FRP tube to twist of the column provided in the equation 4.

$$\text{Relative twist } (\%) = \frac{Column\ twist - FRP\ tube\ twist}{Column\ twist} \times 100 \qquad (4)$$

For column's smaller twists (ie. 0.1° to 0.3°), the relative twist (Fig. 13) was below 20%. The drop in curve at 0.5° twist in Fig. 12 confirmed the cohesion loss between the concrete shell and loading head since FRP tube and concrete shell were in intact with each other during the test. The relative twist reached 40% at 1° twist in the column and continued till 55% at 13.3° twist.

Strain Profile

The vertical and hoop strain along the height of the FRP and steel tubes were shown in Fig. 14. The FRP tube had experienced compression observed from the vertical strain gauge readings in Fig. 14a. The compression force was induced more on FRP tube at surface level of footing due to the diagonal cracks in the concrete. Since the concrete shell and FRP tube rotated as a rigid system, the diagonal cracks on the concrete shell induces stress on the FRP tube. The stress resultant in vertical direction provided compression. This results a vertical strain of 950μ on compression side at the surface level of footing whereas 380μ on tension side at 20 in. (508 mm). At higher twists in the column, the confinement effect on the concrete shell was evident through the hoop strain readings on the FRP tube shown in Fig. 14b. The confinement effect decreased with away movement from the surface of the footing along the height. The variation in confinement was not significant with 480μ hoop strain on FRP at 25 in. (635 mm) location and 1120μ hoop strain on FRP at surface of the footing. Since, the diagonal cracks on concrete shell are not significantly developed resulted in small hoop strain on FRP tube.

At 13.3° twist in the column, the vertical strain gauge located at surface level of the footing showed yielding in the steel tube (Fig. 14c). The yielding was not uniform on all sides of the steel tube. The non-uniformity in readings of vertical steel strain gauges were

due to local deformations in the steel tube and the component of applied torque in vertical direction. However, the vertical steel strain at 20 in. (508 mm) from the surface of the footing was almost zero indicating the friction was low compared to footing surface level. At 13.3° twist in the column, the hoop strain reached 50% of the yield strain of the steel tube at surface level of the footing (Fig. 14d). The higher steel hoop strain value at the surface of the footing on the steel tube indicates friction was exerted between the steel tube and concrete and steel tube was experiencing some fixation at the bottom of the footing against the torsion loading. The strain profile on the cross-section at 13.3° column's twist located at the surface level of the footing was shown in Fig. 15. It was evident that the small deformed shape in the steel tube caused friction inequalities during the test.

The shear strain on the steel tube at heights of 5 in. (127 mm) and 10 in. (254 mm) from the surface of the footing were shown in the Fig. 16. The shear strain on steel tube at surface level of the footing was 800μ which was far below the yield shear strain of 2800μ calculated using on yield stress, yield strain, and Young's modulus (Gere and Timoshenko 1997).

Comparison of Torsion Behavior with RC Column from Previous Studies

Prakash (2009) had investigated the reinforced concrete columns with diameter of 24 in. (610 mm) representing height-to-diameter ratio of 6. The transverse (spiral and hoop) reinforcement ratio of 0.73% with 2.75 in. (70 mm) spacing was investigated. The comparison showed both the HC-FCS and RC columns gained early stiffness. However, the reinforced concrete columns with both spiral and hoop reinforcement started strength reduction at 3° twist in the column whereas the HC-FCS column maintained strength till

13.3° twist in the column. The reinforced concrete columns lost 50% of its ultimate torque at 12° twist of the column whereas the HC-FCS column has 95% of the ultimate torque at 12° twist in the column (Fig. 17).

Summary and Conclusions

The torsional behavior of hollow-core FRP-concrete-steel (HC-FCS) column had been investigated in the current paper. The HC-FCS column consists of 24 in. (610 mm) outer diameter with an aspect ratio of 4. The HC-FCS column consists of concrete shell sandwiched between outer FRP tube and inner steel tube. The FRP tube was placed on the surface of the footing and steel tube was embedded to a length of 1.8 times the diameter of the steel tube. The HC-FCS column's longitudinal and transverse reinforcement was provided in the form of steel tube.

1. The torsional behavior of the HC-FCS column depends on the steel tube's stiffness and the friction existed between the steel tube and concrete.
2. The stiffness of the HC-FCS column maintained even at larger rotations and exhibited good ductility. The FRP tube contribution towards the torque was negligible and confinement to the concrete core was small.
3. The HC-FCS column showcased higher ductility and reached 13.3° rotation without loose in strength compared to reinforced concrete column with loss of 50% in strength at 12.5° rotation with same cross-section.

Acknowledgement

This research was conducted by Missouri University of Science and Technology. In kind contribution from ATLAS Tube is appreciated. Discounts on FRP tubes from Grace Composites and FRP Bridge Drain Pipe are also appreciated. The authors also extend their appreciation to the National University Transportation Center (NUTC) at Missouri University of Science and Technology (Missouri S&T). However, any opinions, findings, conclusions, and recommendations presented in this paper are those of the authors and do not necessarily reflect the views of the sponsors.

Reference

Abdelkarim, O. and ElGawady, M. "Behavior of Hybrid FRP-Concrete-Steel Double-Skin Tubes Subjected to Cyclic Axial Compression." *ASCE Structures Congress 2014a*: pp. 1002-1013.

Abdelkarim, O. and ElGawady, M. "Analytical and Finite-Element Modeling of FRP-Concrete-Steel Double-Skin Tubular Columns." *Journal of Bridge Engineering*, Vol. 20, 2014b.

Abdelkarim, O. and ElGawady, M. "Analysis of Innovative Hollow-Core FRP-Concrete-Steel Columns." *Transportation Research Board (TRB) conference (2015)*, Washington Dc, 15-4430.

Abdelkarim, O., Gheni, A., Anumolu, S., and ElGawady, M. "Seismic Behavior of Hollow-Core FRP-Concrete-Steel Bridge columns." *ASCE Structures Congress*, 2015, pp. 585-596.

Beck, J., and Kiyomiya, O. "Fundamental pure torsion properties of concrete filled circular steel tubes." *J. Materials, Conc. Struct. Pavements*, V-60, No. 739, 2003 pp. 85–96.

Dai, J.G., Yu, L.B., and Teng, J.G. "Behavior and Modeling of Concrete Confined with FRP Composites of Large Deformability." *Journal of Composites for Construction,* Vol. 15, No. 6, 2011, pp. 963-973.

Dawood, H., ElGawady, M., and Hewes, J. "Behavior of Segmental Precast Post-Tensioned Bridge Piers under Lateral Loads". *Journal of Bridge Engineering*, Vol. 17, No. 5, 2012, pp. 735-746.

Dawood, H., ElGawady, M." Performance-based seismic design of unbonded precast post-tensioned concrete filled GFRP tube piers." *Composites Part B: Engineering*, Vol. 44, No. 1, 2013, pp. 357-367.

ElGawady, M., Booker, A., and Dawood, H. "Seismic Behavior of Posttensioned Concrete-Filled Fiber Tubes." *J. Compos. Constr*., Vol. 14, No. 5, 2010, pp. 616-628.

Fam, A., Bart, F., and Sami, R. "Experimental and analytical modeling of concrete-filled FRP tubes subjected to combined bending and axial loads." *ACI Struct. J.,* Vol. 100, No. 4, 2003, pp. 499-509.

Gere, J., M., and Timoshenko, S., P. Mechanics of materials. 1997.

Han, L.H., Yao, G.H., and Tao, Z. "Performance of concrete-filled thin-walled steel tubes subjected to pure torsion." *Thin-Walled Struct*; Vol. 45, No. 1, 2007, pp. 24–36.

Huang, H., Han, L. H., and Zhao, X. "Investigation on concrete filled double skin steel tubes (CFDSTs) under pure torsion." *Journal of Constructional Steel Research*, Vol. 90, pp. 221-234.

Lam, L., and Teng, J.G. "Ultimate condition of fiber reinforced polymer-confined concrete." *Journal of Composites for Construction* Vol. 8, No. 6, 2004, pp. 539-548.

Lee, E., Yun, B., Shim, H., Chang, K., and Lee, G. "Torsional behavior of concrete-filled circular steel tube columns." *J. Structural Engineering,* Vol. 135, No. 10, 2009, pp. 1250-1258.

Mirmiran, A., and Shahawy, M. "A new concrete-filled hollow FRP composite column." *Composites Part B: Engineering*, Vol. 27, No. 3, 1996, pp. 263-268.

Mirmiran, A., Mohsen S., and Thomas B. "Slenderness Limit for Hybrid FRP-Concrete Columns." *Journal of Composites for Construction*, Vol. 5, No. 1, 2001. pp. 26-34.

Montague, P. "Experimental behavior of double-skinned, composite, circular cylindrical-shells under external-pressure." *Journal of Mechanical Engineering Science*, Vol. 20, No. 1, 1978, pp. 21–34.

Moon, J., Lehman, D., Roeder, C., and Lee, H. "Strength of Circular Concrete-Filled Tubes with and without Internal Reinforcement under Combined Loading." *J. Structural Engineering*, Vol. 139, No. 12, 2013.

Nie, J.G., Wang, Y.H., and Fan, J.S. "Experimental study on seismic behavior of concrete filled steel tube columns under pure torsion and compression–torsion cyclic load." *Journal of Constructional Steel Research*, Vol. 79, 2012, pp. 115–126.

Ozbakkaloglu, T., and Akin, E. "Behavior of FRP-confined normal-and high-strength concrete under cyclic axial compression." *Journal of Composites for Construction*, Vol. 16, No. 4, 2011, pp. 451-463.

Ozbakkaloglu, T. "Axial Compressive Behavior of Square and Rectangular High-Strength Concrete-Filled FRP Tubes." *Journal of Composites for Construction*, Vol. 17, No. 1, 2012, pp. 151-161.

Otuska, H., Takeshita, E., Yabuki, W., Wang, Y., Yoshimura, T., and Tsunomoto, M. "Study on the seismic performance of reinforced concrete columns subjected to torsional moment, bending moment and axial force." *World Conference on Earthquake Engineering*, 2004.

Prakash, S.S., Belarbi, A., You, Y.M. "Seismic performance of seismic RC columns subjected to axial force, bending, and torsion with low and moderate shear." Engineering Structures, Vol. 32, No.1, pp. 46-59.

Teng, J.G., Yu, T., and Wong, Y.L. "Behavior of Hybrid FRP-Concrete-Steel Double-Skin Tubular Columns." *Proc. 2nd Int. Conf. on FRP Composites in Civil Engineering*, Adelaide, Australia, 2004, pp. 811-818.

Teng, J. G., Yu, T., Wong, Y. L., and Dong, S. L. "Hybrid FRP concrete-steel tubular columns: Concept and behavior." *Constr. Build. Mater.*, 21(4), 2007, 846–854.

Wong, Y. L., Yu, T., Teng, J. G., and Dong, S. L. "Behavior of FRP-confined concrete in annular section columns." *Composites Part B: Engineering*, Vol. 39, No.3, 2008, pp. 451–466.

Yu, T., Wong, Y., Teng, J., Dong, S., and Lam, E. "Flexural Behavior of Hybrid FRP-Concrete-Steel Double-Skin Tubular Members." J *Journal of Composites for Construction*, Vol. 10, No. 5, 2006, pp. 443–452.

Zhang, B., Teng, J.G., and Yu, T. "Experimental behavior of hybrid FRP–concrete–steel double-skin tubular columns under combined axial compression and cyclic lateral loading." *Engineering Structures*, Vol. 99, 2015, pp. 214-231.

Zhu, Z., Ahmad, I., and Mirmiran, A. "Effect of column parameters on axial compression behavior of concrete-filled FRP tubes." *Advances in Structural Engineering*, Vol. 8, No. 4, 2005, pp. 443-450.

Table 1. Summary of Column Variables

Parameter	**Dimension, in. (mm)**
Outer diameter of column, D	24 (610.0)
Inner diameter of column, d	14 (355.0)
Thickness of FRP tube, t_o	0.45 (11.4)
Thickness of steel tube, t_i	0.25 (6.3)
Embedded length of steel tube, L_e	25 (635.0)

Table 2. Mechanical Proportions of FRP Tube

Material	Axial Compression Elastic Modulus, ksi (GPa)	Ultimate axial Stress, psi (MPa)	Hoop Elastic Modulus, ksi (GPa)	Hoop rupture stress, psi (MPa)
FRP Tube	677 (4.6)	12,150 (83.7)	3,020 (20.8)	40,150 (276.8)

Table 3. Concrete Mixed Proportions

Cement, (lb/yd^3)	Fly Ash, (lb/yd^3)	Fine Aggregate, (lb/yd^3)	Coarse Aggregate, (lb/yd^3)	Water, (lb/yd^3)	w/c ratio	HRWR, (lb/yd^3)
590	170	1,430	1,430	380	0.5	1.9

Table 4. Un-confined Cylindrical Strengths of Concrete

Property	Footing	Column
f'_c, psi (MPa) - 28 days	9,500 (65.5)	5,158 (35.5)
f'_c, psi (MPa) - date of test	9,700 (66.9)	6,910 (51.0)

Table 5. Mechanical Proportions of Steel Tube and Steel Rebar

Property	Yield Stress, psi (MPa)	Elastic Modulus, ksi (GPa)	Ultimate stress, psi (MPa)	Rupture strain
Steel Tube	55,000 (379)	29,000 (200)	68,000 (469)	0.25
Steel Rebar	60,000 (414)	29,000 (200)	90,000 (620)	0.08

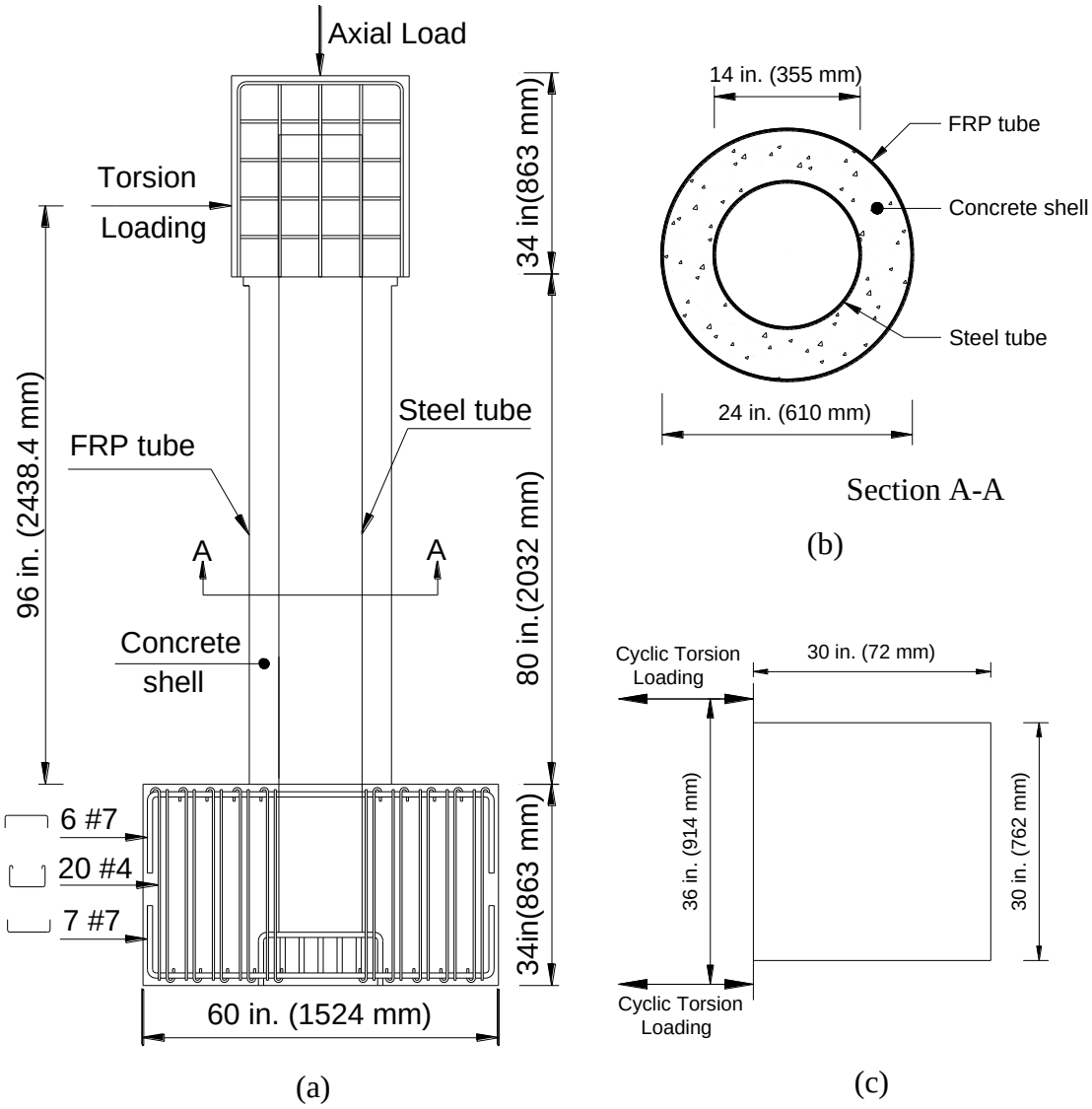

Fig. 1. HC-FCS column (a) Elevation, (b) Cross-section, (c) Plan of Loading Head

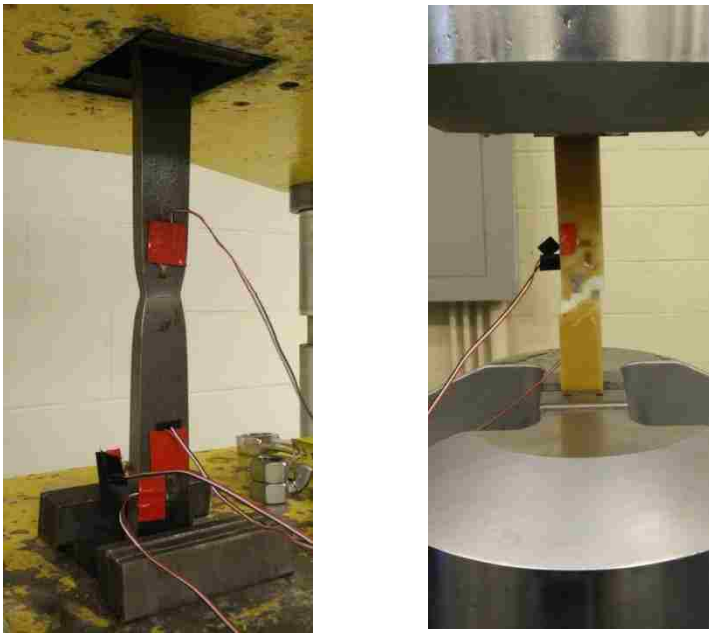

(a) (b)

Fig. 2. Tensile Tests on Coupons (a) Steel, (b) FRP

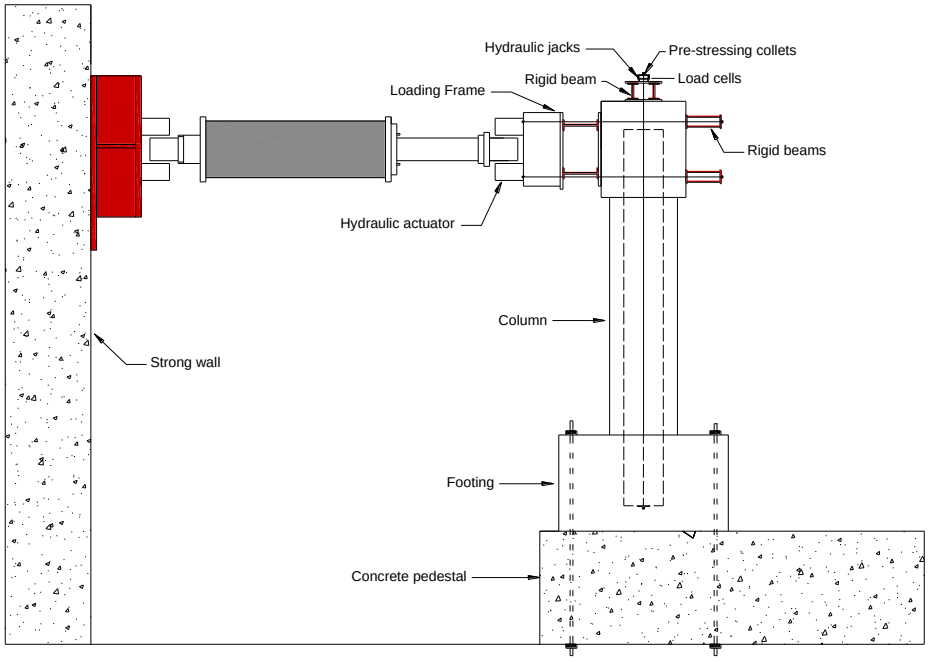

(a)

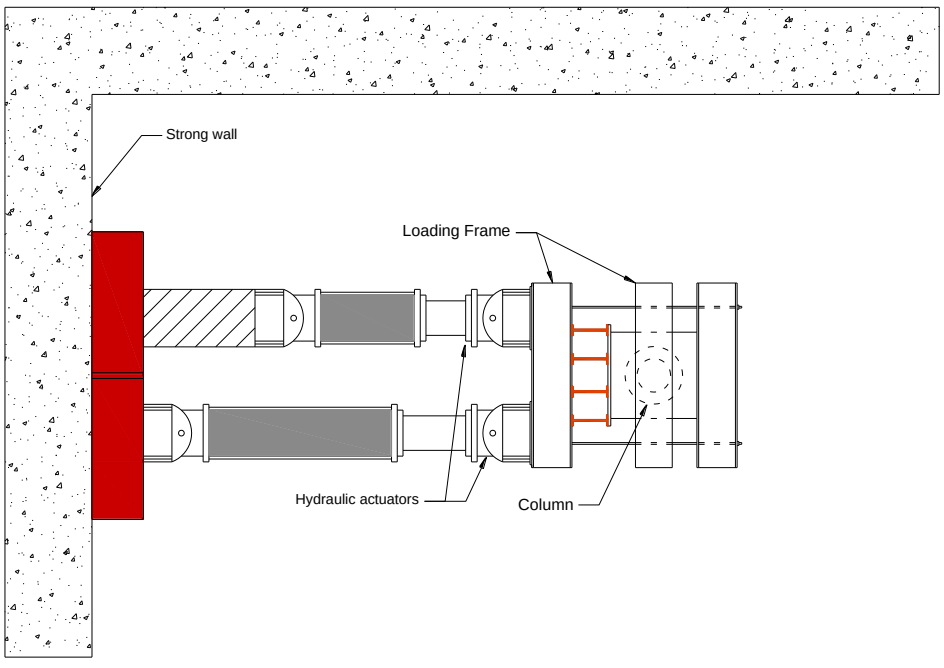

(b)

Fig. 3. Experimental Test Setup (a) Elevation, (b) Plan

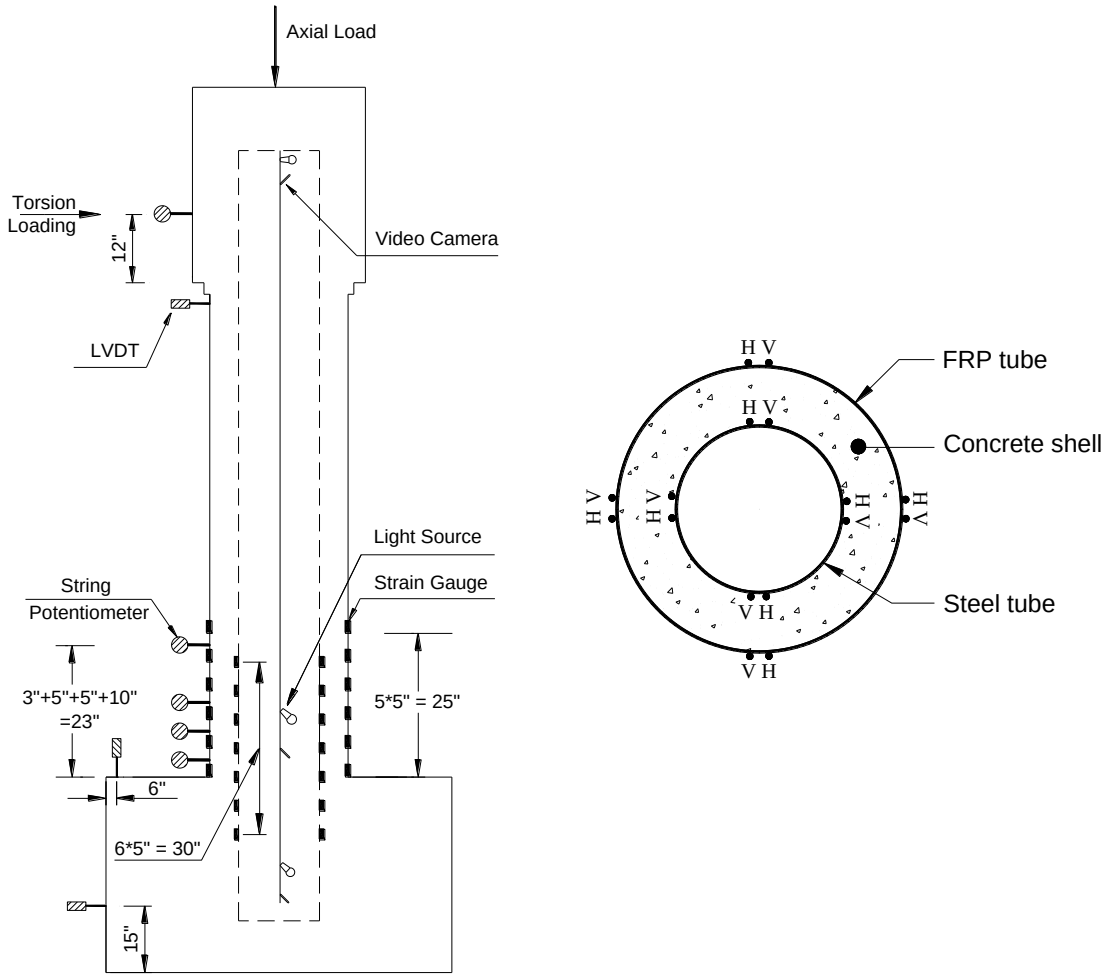

Note: All dimensions are in inches; H- horizontal Strain Gauge; V- vertical strain gauge

Fig. 4. (a) Location of Strain Gauges, LVDT's, and String Potentiometers on the Column; (b) Cross-section of the Column

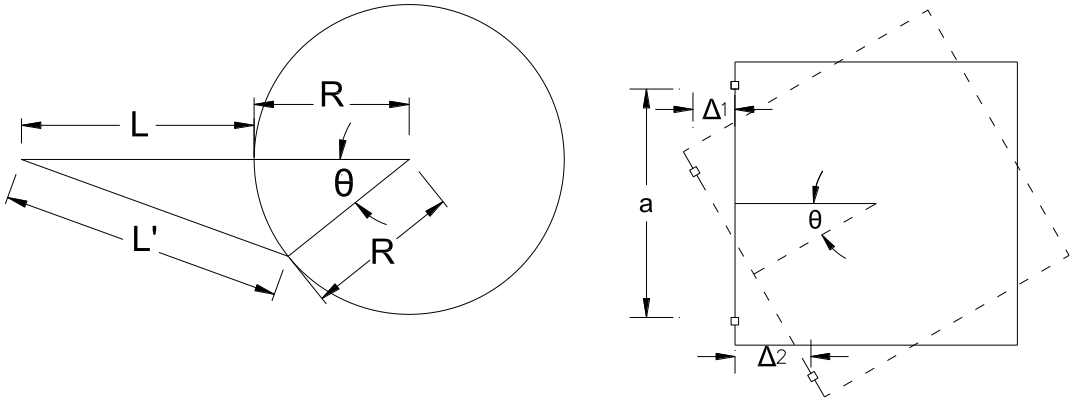

(a) (b)

Fig. 5. Measurement Plan (a) String Potentiometer, (b) LVDT

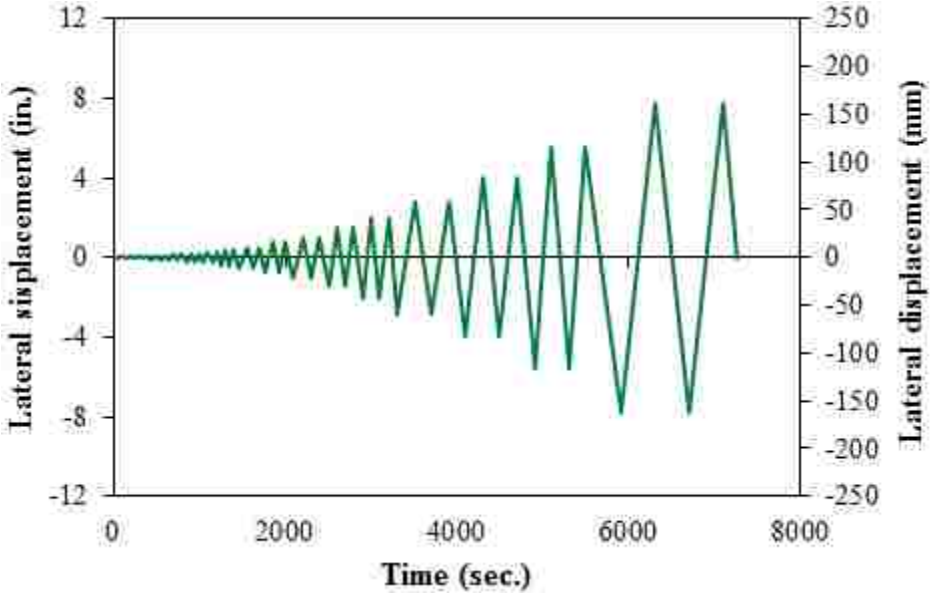

Fig. 6. Loading Regime for Cyclic Torsion Load

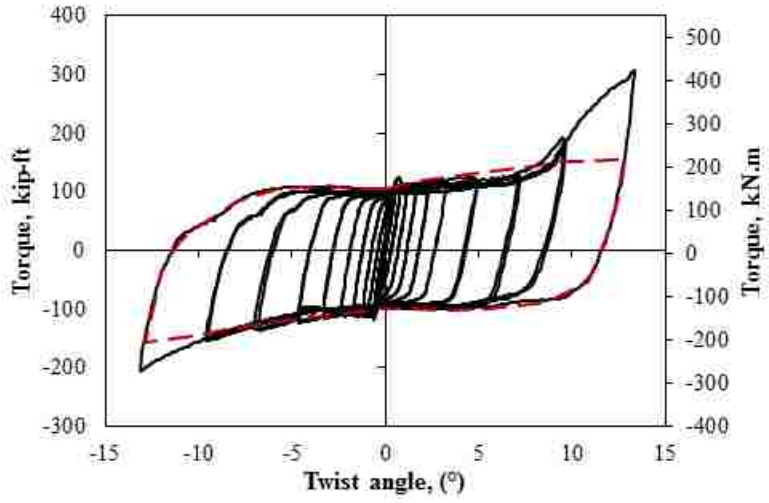

Fig. 7. Torque-Twist Angle of HC-FCS Column under Pure Torsion

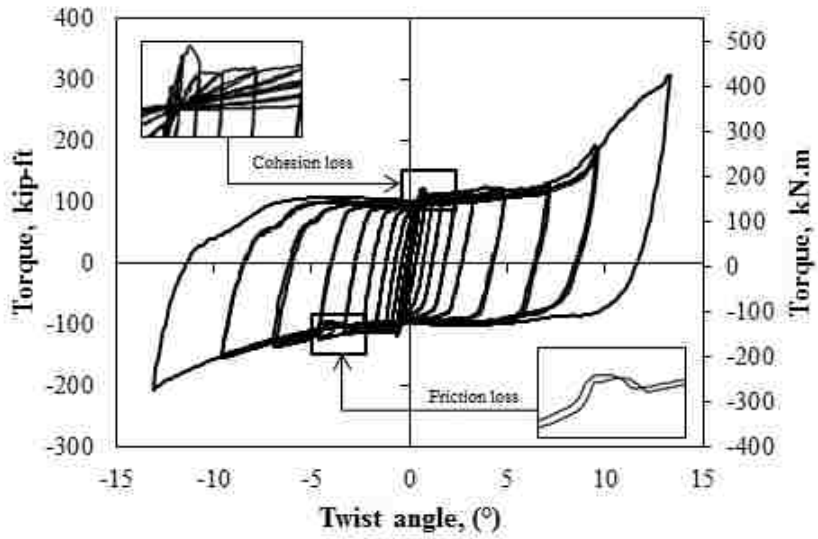

Fig. 8. Friction and Cohesion Effects on Torque-Twist Angle Curve of HC-FCS Column

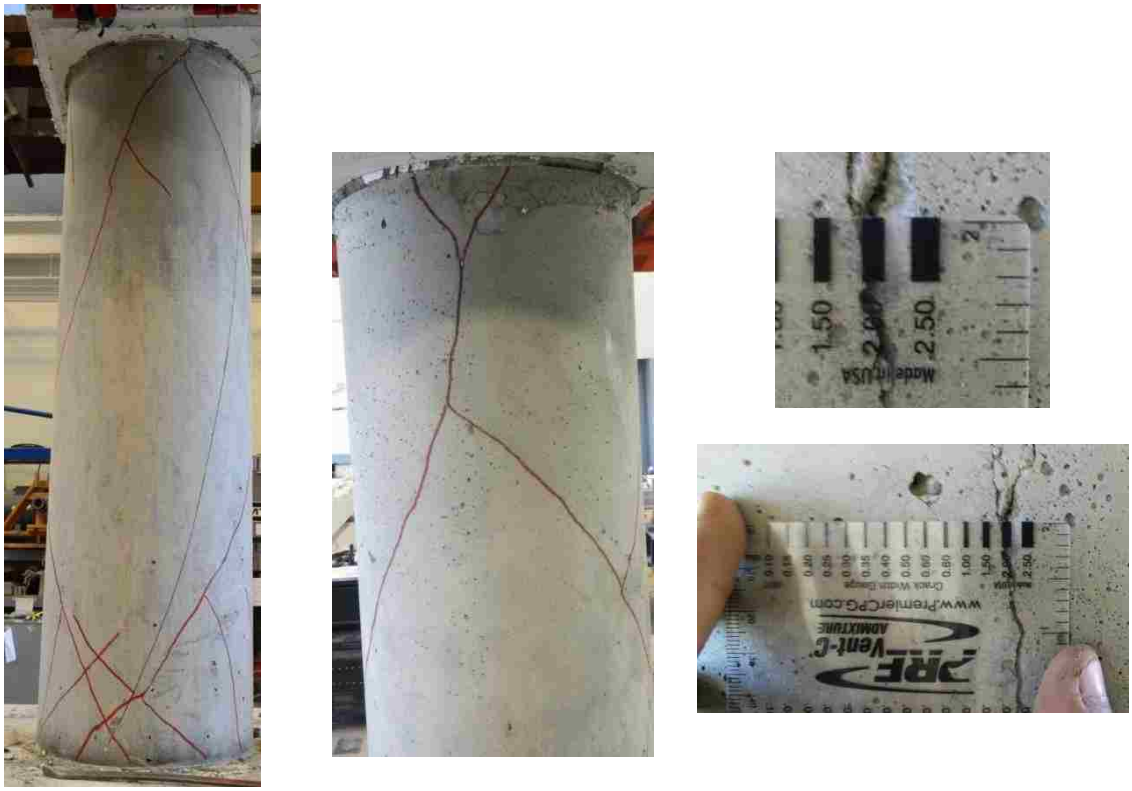

(a) (b) (c)

Fig. 9. Cracks on Concrete Shell (a) North side, (b) South side; (c) Maximum Crack Width on Concrete Shell

(a) (b)

Fig. 10. Grinding of Concrete Surfaces (a) Loading Head, (b) Concrete Shell

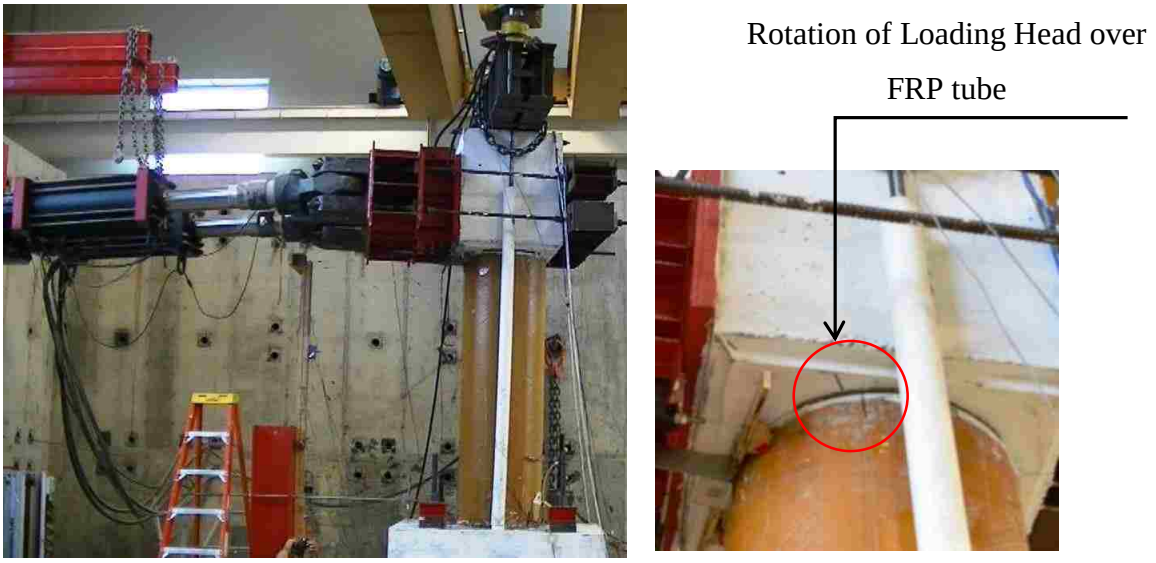

(a) (b)

Fig. 11. Torsional Investigation of HC-FCS Column (a) Elevation View, (b) Slip of Loading Head over FRP Tube at 9° Column Rotation

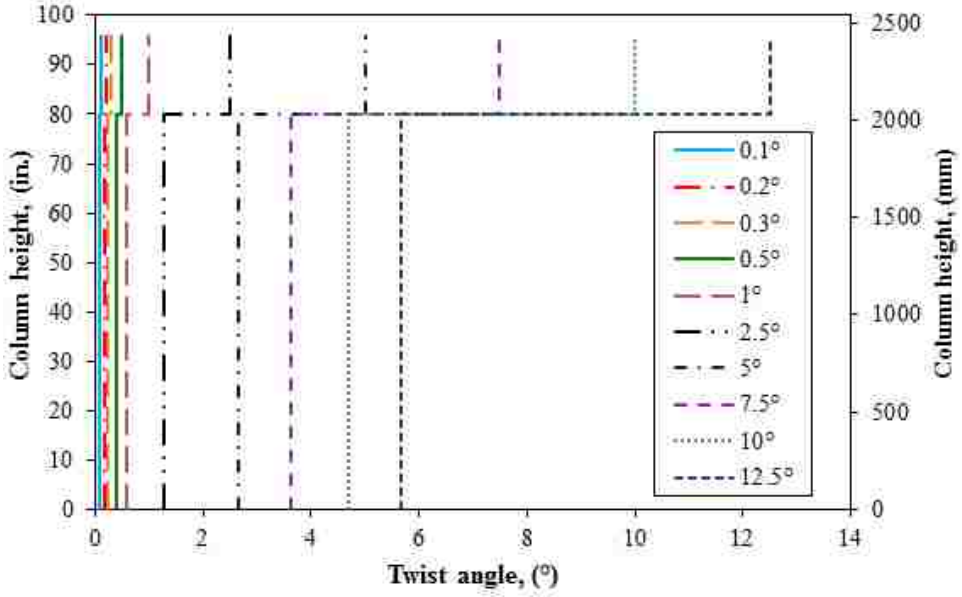

Fig. 12. Variation of Twist Angle along the Column Height

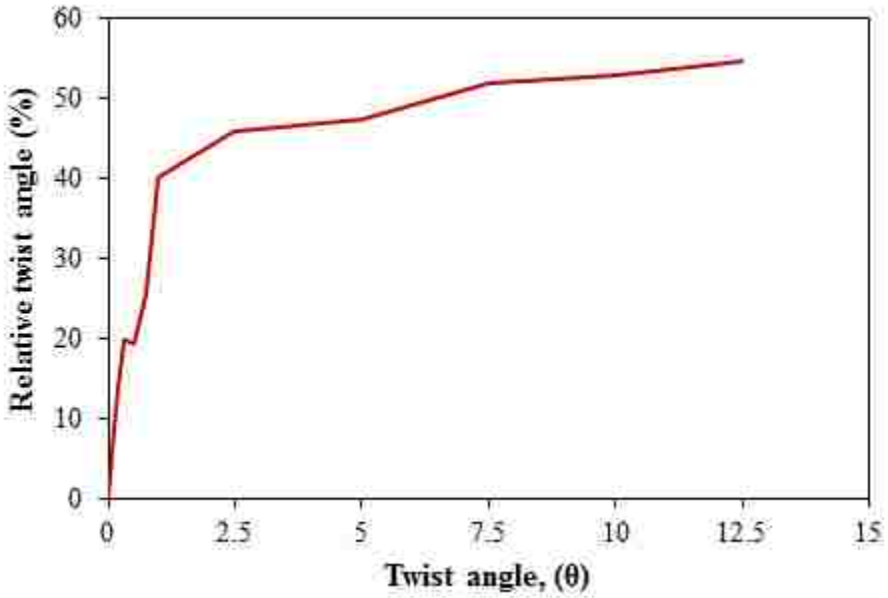

Fig. 13. Relative Twist Angle across Different Twist Angles

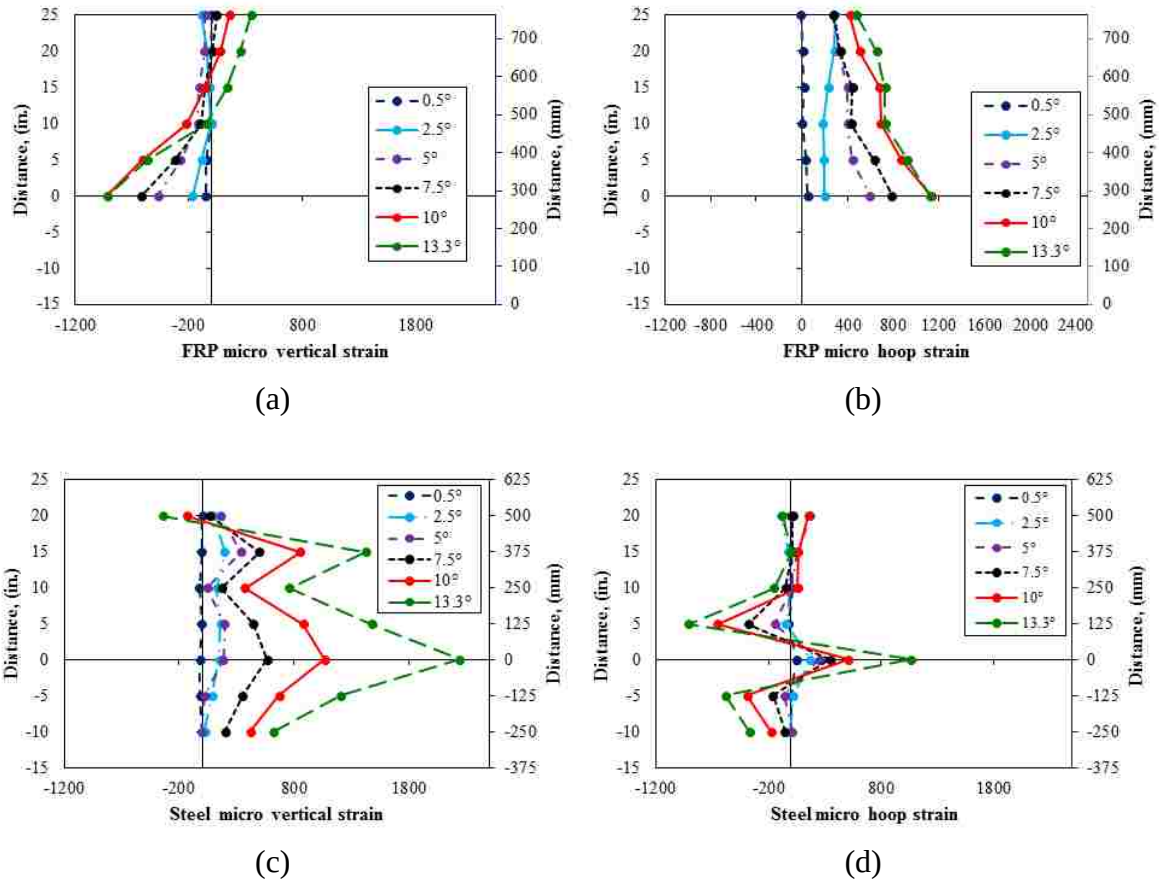

Fig. 14. Strain Gauge Profile along the Height of the Column: (a) FRP Vertical (b) FRP Hoop, (c) Steel Vertical, and (d) Steel Hoop

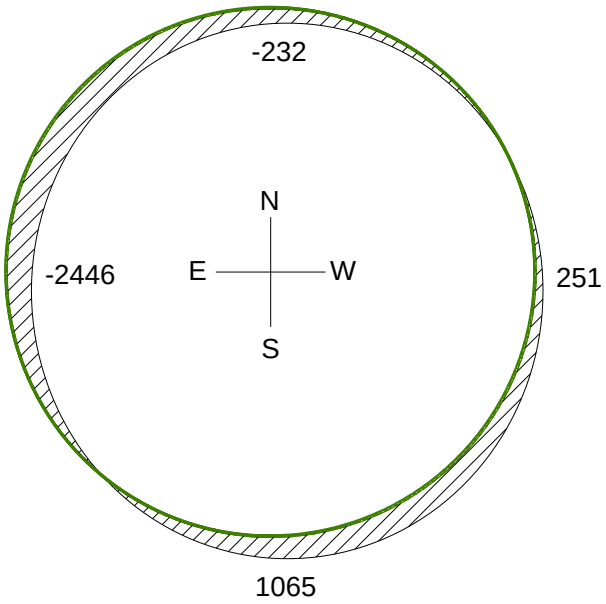

Fig. 15. Hoop Micro Strain Profile on Steel Tube Circumference at 13.3° Column Twist

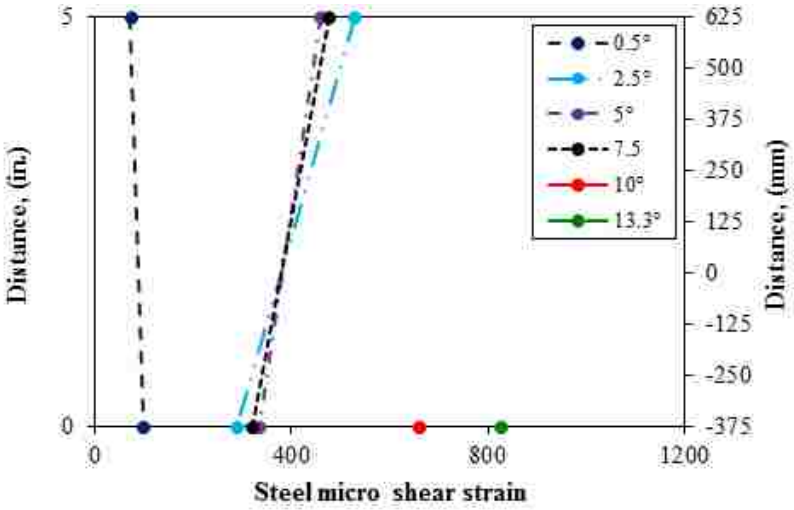

Fig. 16. Shear Strain Profile on the Steel Tube from the Surface of the Footing

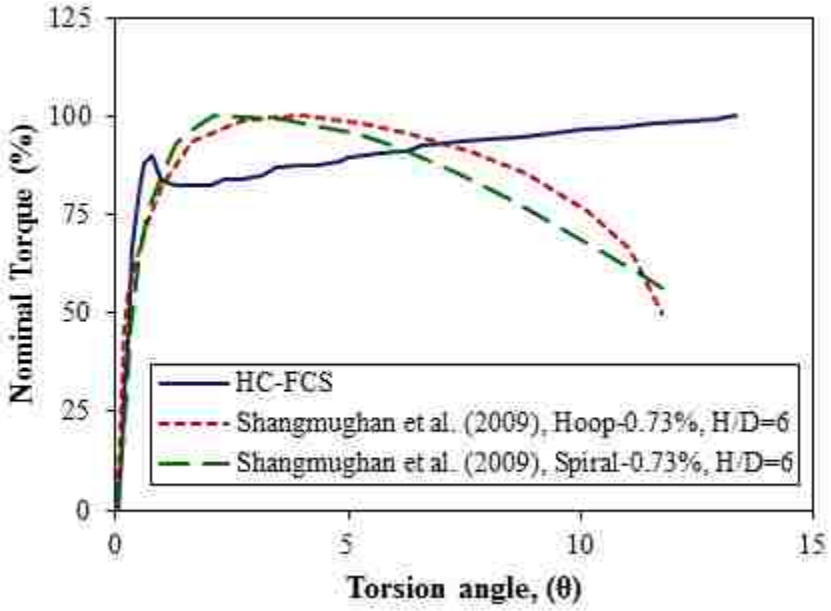

Fig. 17. Comparison of HC-FCS Column and Reinforced Concrete Column from Shanmughan et al. 2009

3. SUMMARY, FINDINGS AND RECOMMENDATIONS FOR FUTURE WORK

3.1. SUMMARY AND FINDINGS

The growth of composite construction over reinforced concrete construction had gained importance especially in seismic region. The dissertation presented the torsional behavior of two types of composite columns namely Hollow-Core Steel-Concrete-Steel (HC-SCS) Columns and Hollow-Core Fiber Reinforced Polymer-Concrete-Steel (HC-FCS) Columns, respectively.

The Ls-Dyna software was used to develop a finite element model for HC-SCS. The HC-SCS consisted of a concrete wall that was sandwiched between steel tubes. The finite element analysis results were validated against experimental results. The proposed model was able to predict the behavior of HC-SCS columns under pure torsion. The Karagozian and Case Concrete Damage Model Release 3 (K&C model), with automatically generated parameters, produced good results for concrete modelling, including the modelling of high strength concrete. Parametric analysis was conducted by assuming the parameters and observing their influence on the T-θ curves. Seven parameters namely strength of steel tubes, strength of concrete shell, diameter-to-thickness ratio of steel tubes, concrete shell thickness, and aspect ratio of the column were studied. The outer steel tube's D/t_o ratio was the governing parameter that controlled the column's torque capacity followed by concrete shell thickness and then the strength of the outer steel tube. The aspect ratio (H/D) of the column and inner steel tube's strength had low influence on the column's torque capacity. All of the six columns had similar failure sequence. The only change in failure was change along the height of

the column. The simplified analytical model developed based on parametric study was good in agreement with the experimental results. The study concluded the following notes.

1. The geometrical and mechanical properties of the outer steel tube significantly influence the torsional behavior of the column.
2. The combination of materials enhances 20% of the column's torsion capacity compared to the individual contribution due to the effect of confinement to the concrete shell and stability to the steel tubes.
3. The inner steel tube's contribution to the column's torsion capacity significantly increased with decrease in concrete shell thickness.

A large-scale HC-FCS column was constructed and experimented under the constant axial and cyclic torsion load. The column's outer diameter was 24 in. (610 mm) with an effective height of 96 in. (2438 mm) from surface of the footing to center point of loading representing an aspect ratio of 4. The FRP tube was stopped at the surface of the footing while the steel tube was embedded into the footing to a length of 1.8 times the diameter of the steel tube. The HC-FCS column's longitudinal and transverse reinforcement was provided in the form of steel tube.

1. The torsional behavior of the HC-FCS column depends on the steel tube's stiffness and the friction existed between the steel tube and concrete.
2. The stiffness of the HC-FCS column maintained even at larger rotations and exhibited good ductility. The FRP tube contribution towards the torque was negligible and confinement to the concrete core was small.

3. The HC-FCS column showcased higher ductility and reached 13.3° rotation with loose in strength compared to reinforced concrete column with loss of 50% in strength at 12.5° rotation at same cross-section.

3.2. RECOMMENDATION FOR FUTURE WORK

The typical torsional behavior of both the HC-SCS and HC-FCS columns were investigated through finite element analysis and experimentation. However, a few further investigations were needed to investigate before the practical use.

1. The significance of shear connecters on HC-FCS needs to be investigated to understand the influence of friction between the contacts.
2. The behavior of HC-FCS column under combined loadings with flexure need to be investigated.
3. Finite element studies on HC-FCS column need to be conducted to study in-detailed behavior.
4. Parametric variation including concrete shell thickness, steel tube thickness, concrete shell thickness, and aspect ratio of the HC-FCS column need to be investigated.
5. The infill concrete in the steel tube of HC-FCS needs to be investigated.
6. A large scale investigation on HC-SCS was necessary with different parameters to study the torsion behavior.

REFERENCES

Abdelkarim, O. and ElGawady, M. (2014a). Behavior of Hybrid FRP-Concrete-Steel Double-Skin Tubes Subjected to Cyclic Axial Compression. ASCE Structures Congress 2014: pp. 1002-1013.

Abdelkarim, O. and ElGawady, M. (2014b) "Analytical and Finite-Element Modeling of FRP-Concrete-Steel Double-Skin Tubular Columns." *Journal of Bridge Engineering*, Vol. 20.

Abdelkarim, O., Gheni, A., Anumolu, S., and ElGawady, M. (2015) "Seismic. Behavior of Hollow-Core FRP-Concrete-Steel Bridge columns." *ASCE Structures Congress*, 2015, pp. 585-596.

Abbasnia, R., Hosseinpour, F., Rostamian, M., and Ziaadiny, H. (2013). "Cyclic and monotonic behavior of FRP confined concrete rectangular prisms with different aspect ratios." Construction and Building Materials, 40, 118-125.

Bai, Y. L., Dai, J. G., and Teng, J. G. (2013). "Cyclic compressive behavior of concrete confined with large rupture strain FRP composites." Journal of Composites for Construction, 18(1), 04013025.

Beck, J., and Kiyomiya, O. (2003). "Fundamental pure torsion properties of concrete filled circular steel tubes." *J. Materials, Conc. Struct. Pavements*, JSCE No. 739/V-60, pp. 85–96.

Dong, C.X., and Ho, J.C.M. (2012). "Uni-axial behaviour of normal-strength HC-SCS columns with external steel rings." Steel and Composite Structures, Vol. 13, No. 6, pp: 587-606.

Fam, A. Z., and Rizkalla, S. H. (2001). "Behavior of axially loaded concrete-filled circular fiber-reinforced polymer tubes." ACI Structural Journal, 98(3).

Han, L.H., Yao, G.H., and Tao, Z. (2007). "Performance of concrete-filled thin-walled steel tubes subjected to pure torsion." *Thin-Walled Struct*; 45(1):24–36.

Han, L. H., Huang, H., and Zhao, X. L. (2009). "Analytical behaviour of concrete-filled double skin steel tubular (CFDST) beam-columns under cyclic loading". *Thin-walled structures*, 47(6), 668-680.

Han, L. H., Tao, Z., Liao, F. Y., and Xu, Y. (2010). "Tests on cyclic performance of FRP–concrete–steel double-skin tubular columns." *Thin-Walled Structures*, 48(6), 430-439.

Hassanein, M.F., Kharoob, O.F., and Liang, Q.Q. (2013). "Circular concrete-filled double skin tubular short columns with external stainless steel tubes under axial compression." *Thin Walled structures*. Vol 73, pp: 252-263.

Huang, H., Han, L. H., and Zhao, X. (2013). "Investigation on concrete filled double skin steel tubes (CFDSTs) under pure torsion." Journal of Constructional Steel Research, Volume 90, 221-234.

Lam, L., and Teng, J. G. (2004). "Ultimate condition of fiber reinforced polymer-confined concrete." Journal of Composites for Construction, 8(6), 539-548.

Lee, G., Xu, J. S., Gong., A., and Zhang, K. C. (1991). "Experimental studies on concrete filled steel tubular short columns under compression and torsion." *Proc. 3rd Intl. Conf. on Steel-Concrete Composite Construction*, ACSCCS, Fukuoka, Japan, 143–148.

Lee, E., Yun, B., Shim, H., Chang, K., and Lee, G. (2009). "Torsional behavior of concrete-filled circular steel tube columns." *J.Struct. Eng*., 135(10), 1250-1258.

Li, W., Han, L.H., and Chan, T. (2014). "Tensile behaviour of concrete-filled double-skin steel tubular members" *Journal of Constructional Steel Research*, Vol. 99, pp. 35-46.

Lin, M.L., and Tsai, K.C. (2001). "Behavior of double-skinned composite steel tubular columns subjected to combined axial and flexural Loads." *Proceedings of the First International Conference on Steel and Composite Structures*, Pusan, Korea, pp. 1145–1152.

Lu, H., Zhao, X., and Han, L.H. (2010). "Testing of self-consolidating concrete-filled double skin tubular stub columns exposed to fire" *Journal of Constructional Steel Research*, Vol. 66, Issues 8–9, pp. 1069-1080.

Mander, J. B., Priestley, M. J. N., and Park, R. (1983). "Behaviour of ductile hollow reinforced concrete columns." Bulletin of the New Zealand National Society for Earthquake Engineering, 16(4), 273-290.

Mirmiran, A., and Shahawy, M. (1996). "A new concrete-filled hollow FRP composite column." Composites Part B: Engineering, 27(3), 263-268.

Nie, J.G., Wang, Y.H., and Fan, J.S. (2012). "Experimental study on seismic behavior of concrete filled steel tube columns under pure torsion and compression–torsion cyclic load." *Journal of Constructional Steel Research*. 79:115–126.

Ozbakkaloglu, T., and Oehlers, D. J. (2008). "Concrete-filled square and rectangular FRP tubes under axial compression." Journal of Composites for Construction, 12(4), 469-477.

Ozbakkaloglu, T., and Fanggi, B. L. (2013). "Axial compressive behavior of FRP-concrete-steel double-skin tubular columns made of normal-and high-strength concrete." *Journal of Composites for Construction*, 18(1).

Ozbakkaloglu, T., and Idris, Y. (2014). "Seismic behavior of FRP-high-strength concrete–steel double-skin tubular columns." *Journal of Structural Engineering*. 140(6).

Qian, J.R. and Liu, M.X. (2008). "Test of seismic of FRP-concrete-steel double-skin tubular columns." *China Civil Engineering Journal*, 41(3), 29-36.

Rousakis, T. (2001). "Experimental investigation of concrete cylinders confined by carbon FRP sheets, under monotonic and cyclic axial compressive load." Research Rep, 1(2).

Shao, Y., Zhu, Z., and Mirmiran, A. (2006). "Cyclic modeling of FRP-confined concrete with improved ductility." Cement and Concrete Composites, 28(10), 959-968.

Tao, Z., Han, L.H., Zhao, and X.L. (2004). "Behaviour of concrete-filled double skin (CHS inner and CHS outer) steel tubular stub columns and beam-columns." *Journal of Constructional Steel* , 60(8), 1129-1158.

Tao, Z., and Han, L. H. (2006). "Behaviour of concrete-filled double skin rectangular steel tubular beam–columns." *Journal of Constructional Steel Research, 62*(7), pp. 631-646.

Teng, J.G., Yu, T., and Wong, Y.L. Behavior of Hybrid FRP-Concrete-Steel Double-Skin Tubular Columns. Proc. 2nd Int. Conf. on FRP Composites in Civil Engineering, Adelaide, Australia, 2004, pp. 811-818.

Teng, J. G., Yu, T., Wong, Y. L., and Dong, S. L. "Hybrid FRP concrete-steel tubular columns: Concept and behavior." *Construction and Building Materials*, 21(4), 2007, 846–854.

Tirasit, P., and Kawashima, K. (2005). "Seismic Torsion Response of Skewed Bridge Piers," *JSCE Journal of Earthquake Engineering*, Tokyo Institute of Technology, Tokyo, Japan, pp. 357-364.

Wei, S., Mau, S.T., Vipulanandan, C., and Mantrala, S.K. (1995). "Performance of new sandwich tube under axial loading: Experiment." *ASCE Journal of Structural Engineering*, Vol. 121, No. 12, pp. 1806-1814.

Xiao. (2004). "Applications of FRP composites in concrete columns." Advances in Structural Engineering, 7(4), 335-343.

Xiao, J. and Zhang, C. (2008). "Seismic behavior of RC columns with circular, square and diamond sections." Construction and Building Materials, Issue 22, 801-810.

Xie, P., Yu, T., Wong, Y. L., and Teng, J. G. (2011). "Compressive Behavior of Large-Scale Hybrid FRP-Concrete-Steel Double-Skin Tubular Columns." *In Advanced Materials Research*, Vol. 243, pp. 1138-1144.

Xu, J. S., Zhou, J., and Lee, G. (1991). "Experimental Studies on Concrete Filled Steel Tubular Medium and Long Columns under Compression and Torsion." *Proc. 3rd Intl. Conf. on Steel-Concrete Composite Construction*, ACSCCS, Fukuoka, Japan, 159–164.

Yu. T. (2007). "Behavior of hybrid FRP-concrete-steel double-skin tubular columns." PhD thesis, The Hong Kong Polytechnic University.

Yu, T., Wong, Y. L., and Teng, J. G. (2010). "Technical Papers: Behavior of hybrid frp-concrete-steel double-skin tubular columns subjected to eccentric compression." *Advances in Structural Engineering*, 13(5), 961-974.

Yu, T., and Teng, J. G. (2010). "Design of concrete-filled FRP tubular columns: provisions in the Chinese technical code for infrastructure application of FRP composites." Journal of Composites for Construction.

Yu, T., and Teng, J. G. (2012). "Behavior of hybrid FRP-Concrete-Steel double-skin tubular columns with a square outer tube and a circular inner tube subjected to axial compression." *Journal of Composites for Construction*, 17(2), 271-279.

Zahn, F. A., Park, R., and Priestley, M. J. N. (1990). "Flexural strength and ductility of circular hollow reinforced concrete columns without confinement on inside face." ACI Structural Journal, 87(2).

Zhang, B. S., Yu, T., and Teng, J. G. (2011). "Axial compression tests on hybrid double-skin tubular columns filled with high strength concrete." *3rd International Postgraduate Conference on Infrastructure and Environment.*

Zhao, X.L., Han, B., and Grzebieta, R.H. (2002). "Plastic mechanism analysis of concrete-filled double-skin (SHS inner and SHS outer) stub columns." *Thin-Walled Structures*; 40(10): 815–33.

Zhao X.L. and Han L.H. (2006). "Double skin construction", *Progress in Structural Engineering and Materials*, Vol.8, No.3, 93-102.

VITA

Sujith Anumolu was born on July 23rd, 1992 in Vijayawada, India. In 2013, he received his Bachelor of Engineering (B.E) degree in Civil Engineering from Andhra University, India. In May 2016, he received his Master of Science (M.S) degree in Civil Engineering with Structural as emphasis from Missouri University of Science and Technology, Rolla, USA.